Title
DETERMINATION OF n-MESON MASSES BY NEUTRON TIME OF FLIGHT

Author
Czirr, John B.

Publication Date
1962-02-19

UCRL 9951

University of California

Ernest O. Lawrence Radiation Laboratory

DETERMINATION OF π-MESON MASSES BY NEUTRON TIME OF FLIGHT

Berkeley, California

DISCLAIMER

UCRL-9951
Errata
Physics UC-34
TID-4500 (17th Ed.)

UNIVERSITY OF CALIFORNIA
Lawrence Radiation Laboratory
Berkeley, California

September 17, 1962

ERRATA

TO: All recipients of UCRL-9951, Physics distribution

FROM: Technical Information Division

Subject: Determination of π-Meson Masses by Neutron Time of Flight, by John B. Czirr (Ph. D. Thesis), February 19, 1962.

Please make the corrections on subject report as indicated on the attached sheet.

UCRL 9951 ERRATA

Page	v (line 5)	$m_{\pi^-} = 139.69 \pm .41$ MeV/c^2
	v (line 7)	$m_{\pi^-} - m_{\pi^o} = 4.6056 \pm .0055$ MeV/c^2
	v (line 9)	$(8.0 \pm 1.5) \times 10^6$ cm sec.
	7	(Ref. 8) in caption, not (Ref. 19).
	18	Caption should read: Neutron counter resolution at 17 ft. for slow-neutron pulse height.
	19	Caption should read: Neutron counter resolution at 17 ft. for π^o-decay γ pulse height.
	26	13 counts from +25 to +30 mm (not 8 counts).
	29 (line 1)	Should read time distribution, not velocity distribution.
	31	Cut data off at -65 mm.
	33 (line 20)	Should read: vs not us .
	43 (Table II)	Change γ-n separation error from 0.36 to 0.60 for 400-kev neutron run at 67 ft.
	45 (line 3)	Should be velocity, not veloctiy.
	45 (line 20)	$S_\Delta = 0.0065$ MeV/c^2 not 0.0031 MeV/c^2.
	45 (line 22)	$\Delta = 4.6056 \pm .0055$ MeV/c^2.
		Note: For a revision of Table II which leads to these errors see: J.B. Czirr, Determination of π-Meson Masses by Neutron Time of Flight (to be published).
	46 (line 8)	$S_{m_{\pi^-}} = 0.41$ MeV/c^2.
	48 (line 23)	$(8.0 \pm 1.5) \times 10^6$ cm/sec not $(8.7 \pm .7) \times 10^6$ cm/sec.
	48 (line 26)	$m_{\pi^-} - m_{\pi^o}$ is $4.6056 \pm .0055$ MeV/c^2.
	49 (line 12)	m_{π^-} is $139.69 \pm .41$ MeV/c^2.
	49 (line 15)	$(8.0 \pm 1.5) \times 10^6$ cm/sec not $(8.7 \pm .7) \times 10^6$ cm/sec.

UCRL-9951
UC-34 Physics
TID-4500(17th Ed.)

UNIVERSITY OF CALIFORNIA

Lawrence Radiation Laboratory
Berkeley, California

Contract No. W-7405-eng-48

DETERMINATION OF π-MESON MASSES BY NEUTRON TIME OF FLIGHT

John B. Czirr

(Ph. D. Thesis)

February 19, 1962

Printed in USA. Price $1.50. Available from the
Office of Technical Services
U. S. Department of Commerce
Washington 25, D.C.

DETERMINATION OF π-MESON MASSES BY NEUTRON TIME OF FLIGHT

Contents

DETERMINATION OF π-MESON MASSES BY NEUTRON TIME OF FLIGHT

John B. Czirr

Lawrence Radiation Laboratory
University of California
Berkeley, California

February 19, 1962

ABSTRACT

Time-of-flight techniques were used to measure the velocities of the neutrons from the reactions, at rest, $\pi^- + p \rightarrow n + \pi^0$ and $\pi^- + p \rightarrow n + \gamma$. From these velocities the π^- mass and the $\pi^- - \pi^0$ mass difference were obtained, yielding the values

$$m_{\pi^-} = 139.69 \pm .141 \text{ Mev}/c^2$$

and

$$m_{\pi^-} - m_{\pi^0} = 4.6064 \pm .0055 \text{ Mev}/c^2.$$

The velocity distribution about the mean velocity was measured and found to have an rms deviation of $(8.0 \pm 1.5) \times 10^6$ cm/sec.

Negative π mesons from the Lawrence Radiation Laboratory 184-inch synchrocyclotron were degraded by 33 g/cm^2 of carbon and stopped in a 1-in.-high liquid hydrogen target. The neutrons were detected in a 1-in.-thick plastic scintillator viewed by seven RCA 7046 photomultiplier tubes. Neutron times of flight were measured over distances of 17 ft, and 47 ft, and 67 ft. Time was measured for each event from the time of detection of a γ ray associated with that event (one of the γ rays from the reaction $\pi^0 \rightarrow 2\gamma$ in the case of the low-energy neutron). The γ-detector signal was delayed and photographed along with the neutron signal on an oscilloscope trace.

I. INTRODUCTION

A measurement of the velocities of the neutrons arising from stopped negative pions in hydrogen affords a means of accurately determining the π^- mass and the $\pi^- - \pi^0$ mass difference. In both the reactions, at rest

$$\pi^- + p \rightarrow \pi^0 + n \qquad (1)$$

and

$$\pi^- + p \rightarrow \gamma + n, \qquad (2)$$

the final-state neutrons have a unique velocity in the laboratory system which depends only on the rest masses involved. Previous experiments using this method have obtained the most accurate determinations of the $\pi^- - \pi^0$ mass difference to date.[1] Other experiments determined the mass difference by measuring the Doppler shift in the energy[2] or the angular correlation[3] of the γ rays from π^0 decay in order to determine the π^0 velocity. The present value for the mass difference is $4.59 \pm .05$ Mev/c^2.[4]

The most accurate determinations of the $\pi^\pm$ mass are of three types: (a) range-momentum,[5] (b) mesic x-rays,[6] and (c) γ energy from Reaction (2).[7] The combined result of these methods gives the value $m_{\pi^-} = 139.63 \pm .06$ Mev/c^2.[6]

This experiment was undertaken to greatly improve the $\pi^- - \pi^0$ mass-difference determination and to obtain the π^- mass by an independent method with accuracy comparable to the previous values. In addition, deviations about the mean velocity were observable and the velocity distribution of the slow neutrons from Reaction (1) was determined.

II. EXPERIMENTAL TECHNIQUE

For an isotropic source of particles, the fractional error in time of flight is independent of the path length, if the error on the determination of time of arrival varies inversely with the square root of the number of detected events. Under these conditions, there would be no necessity for flight paths longer than those easily available near the source. However, to reduce systematic errors in time-of-flight measurements it is desirable to measure the <u>difference</u> in flight time between two or more positions relative to the source. To reduce the

fractional error in this case it becomes necessary to have the near distance small compared with the far distance.

The closest feasible distance is determined by considerations of background due to the incoming particles (not necessarily decreasing as $1/R^2$ from the target) and differences in flight path from target to detector due to finite target and detector size.

At the Berkeley 184-inch cyclotron, the characteristics of the available beam of π^- mesons require a liquid hydrogen target approximately 1 foot thick in the beam direction in order to stop an acceptable fraction of the particles. For a neutron detector of approximately the same horizontal dimension, a target-counter separation of 10 feet yields a maximum-to-minimum flight-time difference for slow neutrons of approximately 2 nanoseconds because of oblique flight paths. For this reason and because of shielding requirements, the minimum distance from source to neutron detector was set at 10 to 20 feet.

The maximum distance is determined primarily by the minimum useful signal-to-background ratio of the final data. The longest flight path used was 67 feet, at which distance the signal-to-background ratio was approximately unity. For a smaller signal-to-background ratio, it becomes difficult to determine the mean of a peak in the velocity distribution. For depths greater than 67 feet, the signal-to-background ratio is less than unity because of a constant background level in the neutron counter.

Neutron time of flight was measured by displaying the start pulse (γ detector output from $\pi^0 \rightarrow 2\gamma$ in Reaction (1) and the 130-Mev γ from Reaction (2)) and the neutron detector signal on an oscilloscope and photographing the trace. The long time delay between these two events (of the order of microseconds) was compensated for by delaying the γ signal through a low-attenuation delay line.

In order to minimize the spread in flight time of the neutrons, it was necessary to use a liquid hydrogen target thin in the direction along the neutron flight path, and a thin neutron detector. Both of these dimensions were 1 inch in this experiment. The neutron detector consisted of a plastic-organic scintillator viewed by RCA 7046 photomultiplier tubes, thereby yielding time-of-arrival pulses with

intrinsic time spreads of the order of nanoseconds.

III. EXPERIMENTAL EQUIPMENT

To provide the shielding for the neutron detector at all distances, a shielding hole 2 feet in diameter and 150 feet deep was dug near the source of mesons from the cyclotron and lined with a vacuum-tight pipe. The neutron counter was moved vertically in this hole by means of a motor-driven cable drive. The hole was filled with He gas during the experiment to reduce the neutron scattering in the long flight path.

Hydrogen Target and Meson Beam

A liquid hydrogen target 1 ft in diameter and 1 in. high was placed over the time-of-flight hole, in the beam of π^- mesons. This beam was deflected and focused by a bending magnet and two quadrupole magnets and was measured to be 3.5×3.5 in. (full width at half maximum) at the position of the target.

The bending magnet was provided with a pole tip having an 8-in.-high gap which was 24 in. transverse to the beam direction. A 31° wedge was chosen as the pole tip shape in order to focus at the liquid hydrogen target mesons of all momenta entering this magnet. The final quadrupole was placed as close as possible to the liquid hydrogen target in order to minimize the magnification of the cyclotron meson target (object). Both quadrupoles were 8-in.-diameter doublets, and the polarity of both was converging-diverging in the horizontal plane. The length of each element of the first doublet was 8 in. and of the second, 16 in. The experimental setup is shown in Fig. 1.

The liquid hydrogen container was contructed of 5-mil stainless steel. This container was enclosed in a stainless steel pressure dome 20 mils thick, and provided with vents such that the pressure was equal on the inside and outside of the liquid container. This in turn was contained in a vacuum tank with a 38-mil Al bottom dome to permit the neutrons to escape downward. A drawing of the target is shown in Fig. 2. Carbon 33 g/cm^2 thick was placed in front of the target to degrade the beam energy and maximize the number of mesons stopping in the hydrogen.

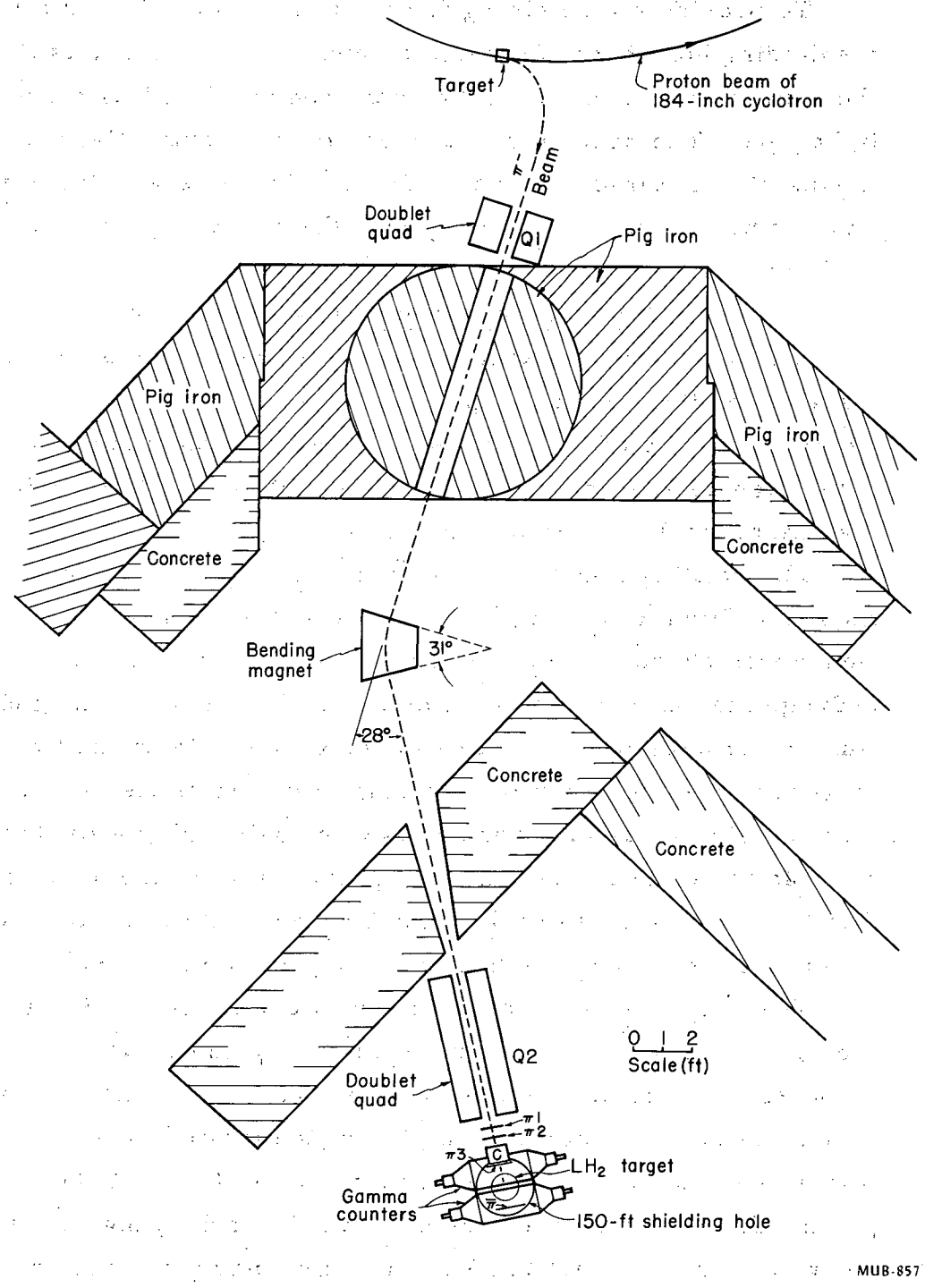

Fig. 1. Meson cave experimental setup.

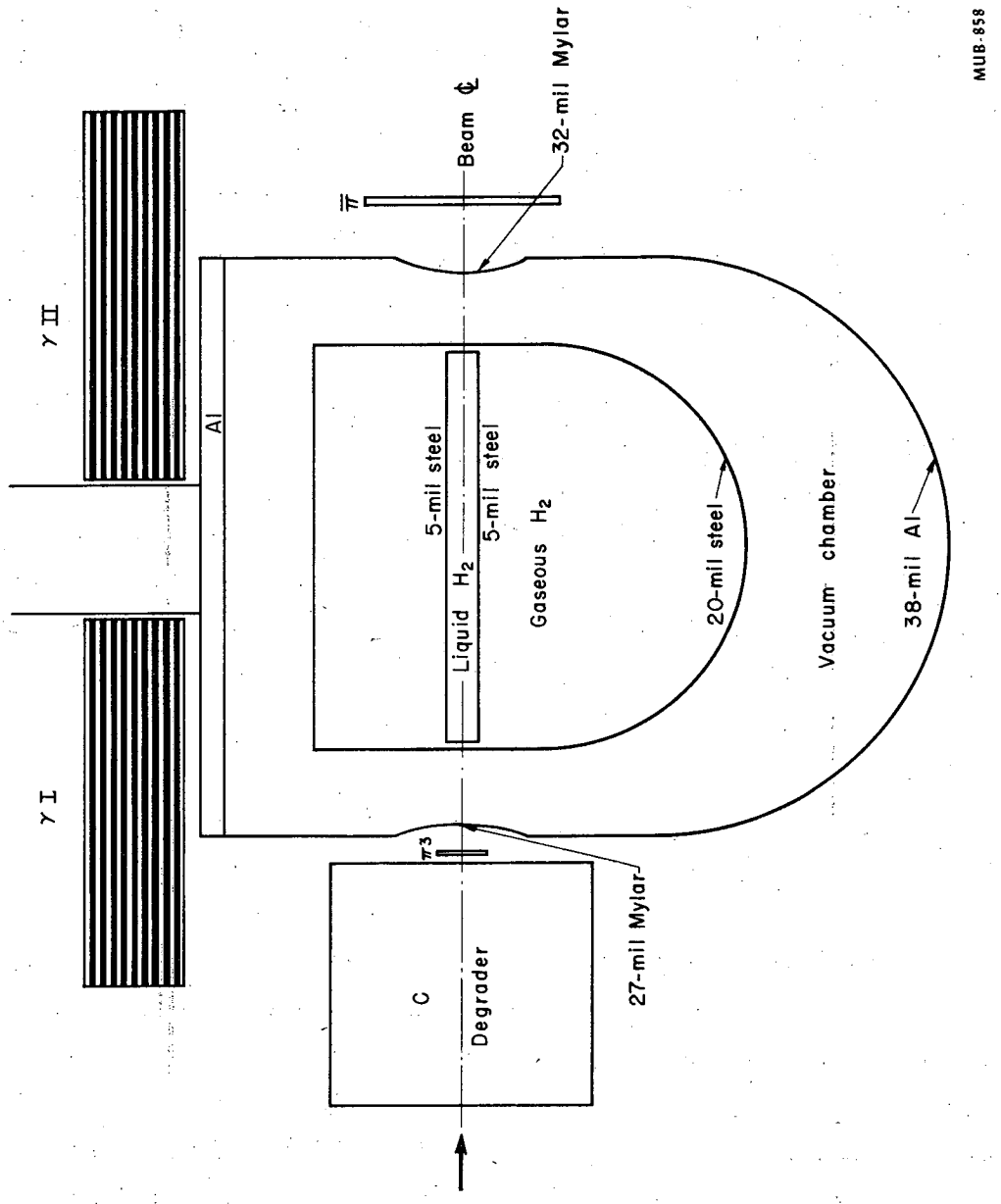

Fig. 2. Liquid hydrogen target and counters.

Electronics

In order to minimize background, a coincidence was required among
(a) the incoming beam monitor,
(b) a γ detector placed above the target, and
(c) two of the neutron-detector phototubes.
The last requirement reduced the background due to phototube dark current to a negligible value. The above coincidence output was used to trigger an oscilloscope which used two traces of a four-trace oscilloscope tube attached to a Tektronix 517A. The sum of all neutron-counter tubes was displayed on one trace and the sum of the γ-counter tubes was displayed on the other. The sweep speed was set at approximately 20 nsec/cm. The oscilloscope face was photographed with a DuMont camera using Tri-X film. A diagram of the electronics is shown in Fig. 3.

a. π Beam Monitor

The π monitor consisted of two $1/4\times6\times12$-in. plastic scintillation counters and one $1/4\times1.5\times10$-in. defining counter, all viewed by RCA 6810A photomultiplier tubes. A $1/4\times6\times11$-in. scintillation counter was placed behind the liquid hydrogen target to detect those particles which did not stop in the target. A $\pi_1\pi_2\pi_3\overline{\pi}$ coincidence was required to obtain a π count.

b. Gamma Counters

The gamma counters consisted of 19 alternate layers of plastic scintillator (10 layers) and lead (9 layers) each of dimensions $1/8\times11\times23$-in. Alternate layers of scintillator were viewed on the $1/8\times11$-in. surface by one RCA 7046 phototube through a polished aluminum (Alzak) light pipe. Only one end of each scintillator was exposed to a phototube so that if necessary, a coincidence could be required between the signals from alternate layers to eliminate heavily ionizing particles. During the experiment this proved unnecessary and signals from the two ends were added together. Two of these counters were placed above the liquid hydrogen target and separated from it by 11 in. The gamma counters subtended approximately 12% of the total solid angle around the target and the calculated

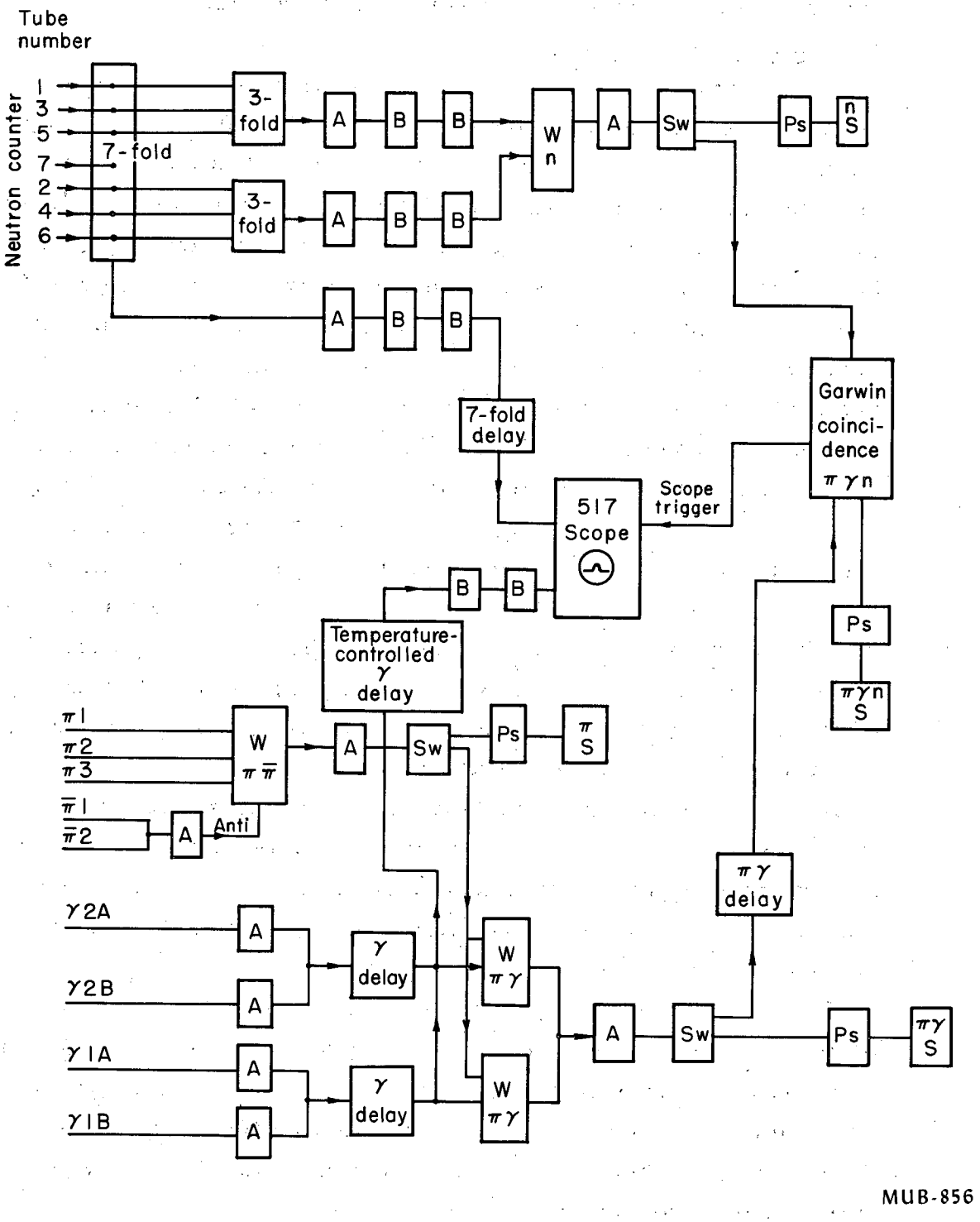

Fig. 3. Diagram of electronics. A and B refer to Hewlett-Packard 460 A and 460 B amplifiers, W to Wenzel coincidence circuits, Sw to Swift discriminators, Ps to Hewlett-Packard 520 A prescalers, and S to scalers. (Ref. ~~19~~ 8)

efficiency of these counters was 80% based upon the thickness of the lead used and the pulse-height spectrum observed.

c. Neutron Counter

The neutron counter consisted of a 1× 15.5-in. disc of UCRL terphenyl-plastic scintillator viewed by 7 RCA 7046 photomultiplier tubes through a 5-in. -thick lucite light pipe. Between the light pipe and the tubes was placed a 1-in. -thick Pb plate with a 3.5-in. hole centered over each tube. One-inch extensions to the large light pipe filled these holes and were optically sealed to the phototube face with Dow-Corning silicone grease. Surrounding the scintillator and phototubes on the sides and bottom was a 1-in. -thick lead shield. Surrounding the sides and top of the phototube volume was a 1/8-in. -thick μ metal magnetic shield. The counter and shields were enclosed in an iron container with an attached refrigerator, the latter for the purpose of reducing dark current from the phototubes. A 20-mil-thick μ metal dome formed the top of the container. The thick light pipe and lead plate served to shield the scintillator from radioactivity (primarily Ra in equilibrium with its decay products) emanating from the phototube glass. The remainder of the lead shield was for the purpose of reducing the detection of background radioactivity originating in the ground surrounding the counter. A drawing of the neutron counter is shown in Fig. 4.

All components inside the lead shield and the shield itself were tested for background radioactivity at the University of California low-background room. The lead chosen was from the St. Joseph lead mine and was found to be well below the average in radioactivity of lead from other sources.

The voltages for each of the seven RCA 7046 phototubes were set to minimize the cathode transit-time spread over a 3.5-in. -diameter circular area centered on the tube face. Outside this region the collection efficiency is very low for this tube type, and masking off the outer region has the primary effect of eliminating infrequent pulses with large transit times.

The transit-time spread over the central region was minimized in the following manner: light pulses from a UCRL pulsed Mercury discharge lamp[8] were attenuated until the frequency of detected

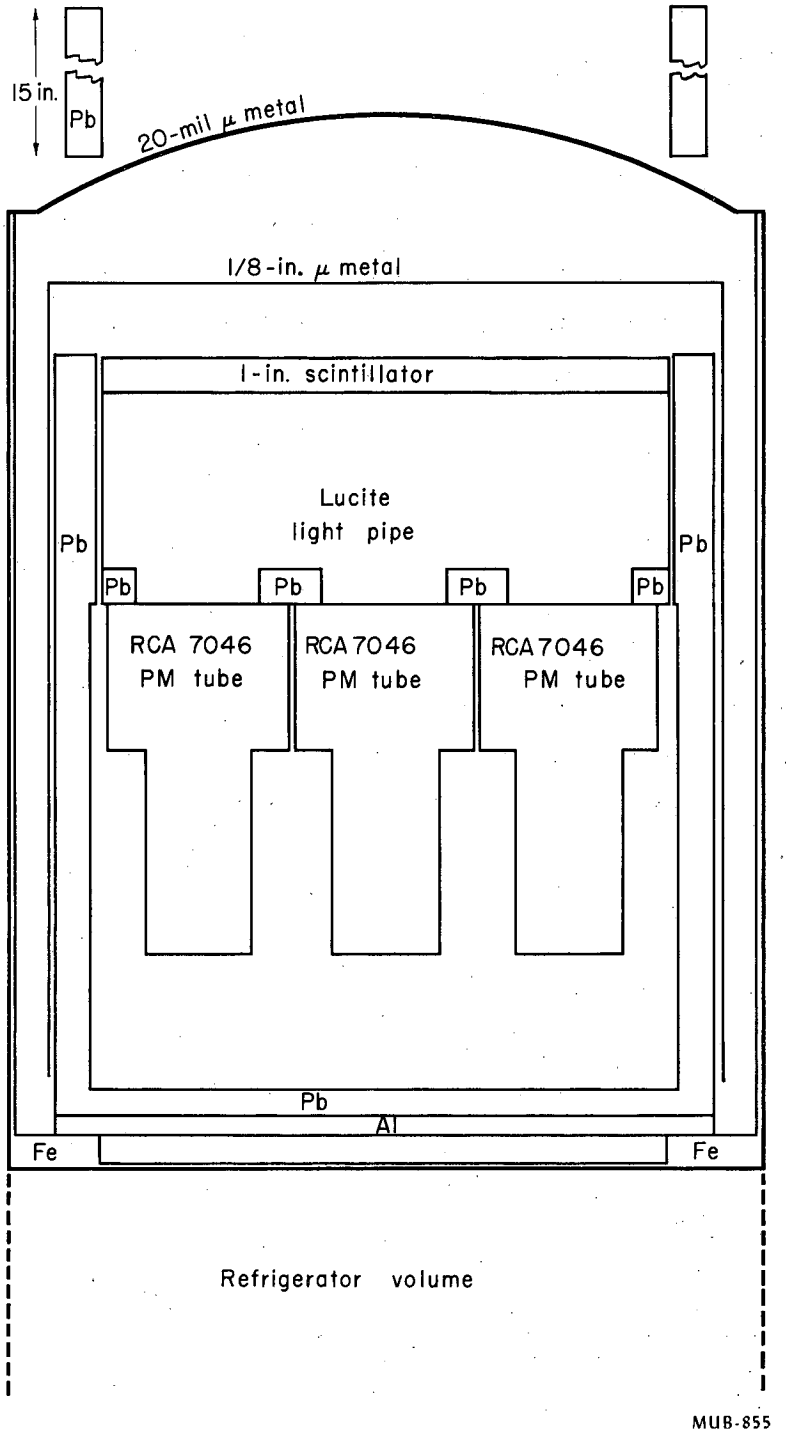

Fig. 4. Neutron counter and shielding.

pulses for a single tube was much lower than the repetition rate of the light source. This assures the condition that essentially only single photoelectrons are being detected. Under these conditions the voltages in the cathode end of the tube were varied until the transit time differences were minimized as observed on an oscilloscope. Then approximately 100 events were photographed and their time spread measured. By repeating this process the minimum spread was obtained from a series of voltage settings. The rms transit-time spread averaged over all seven tubes used was reduced to 3.4 nanoseconds by this technique. This value corresponds to single photoelectrons arriving at the first dynode of the tube. A typical voltage divider is shown in Fig. 5. Because of the high voltages required by the above conditions the dark-current counting rate from the tube was monitored. All tubes were rejected in which a substantial increase in dark counts was detected as the voltages were raised from the values recommended by the manufacturer to the higher voltages. Approximately half of the tubes tested met both the requirements of small transit-time spread and low dark counts. In the assembled counter, the rms time spread was 2.9 nanoseconds averaged over the 400-kev neutron pulse-height distribution. The coincidence detection efficiency for the slow-neutron pulse-height range was 66%, and was 96% for the fast-neutron pulse height. See Section IV for a discussion of these efficiencies.

Neutron-Counter Adders

In order to add the seven phototube signals from the neutron counter, a distributed adder was constructed which gave a linear sum of the seven input signals with a gain of unity for a single input. A diagram of the sevenfold adder is given in Fig. 6. The input signals were lined up with short delay cables in order to minimize the time spread in the output signal. The amplified output of this adder was the signal displayed on the oscilloscope trace. Only one signal cable was available for each tube because of the restricted space available in the shielding hole, so both the coincidence signals used in the trigger and the sevenfold signal were taken from the sevenfold input with a transformer coupling. Alternate tubes in the outer ring were

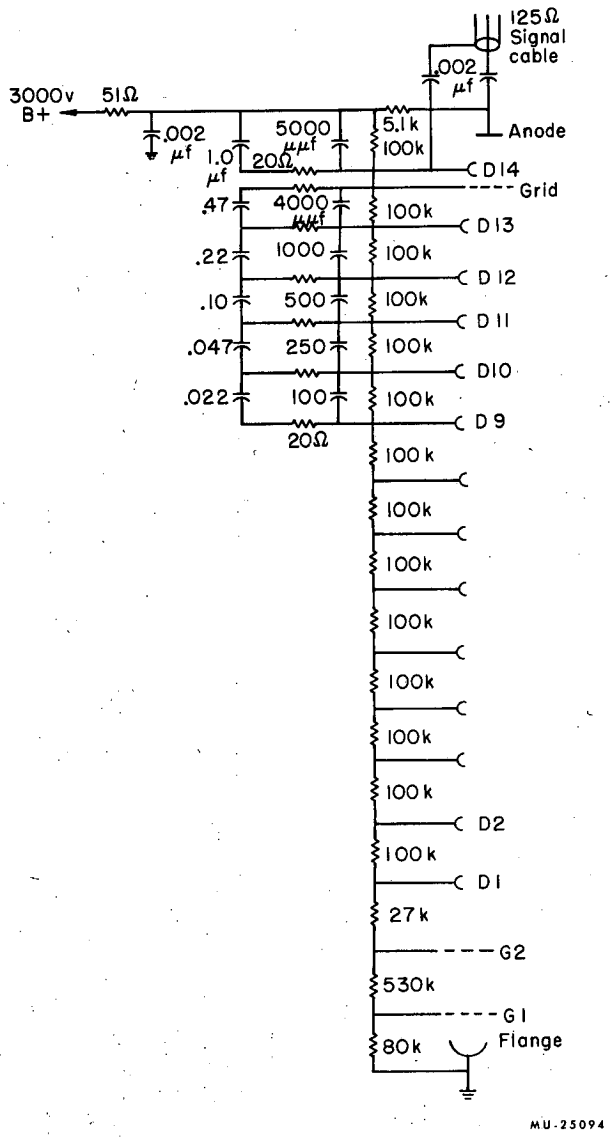

Fig. 5. Typical voltage divider.

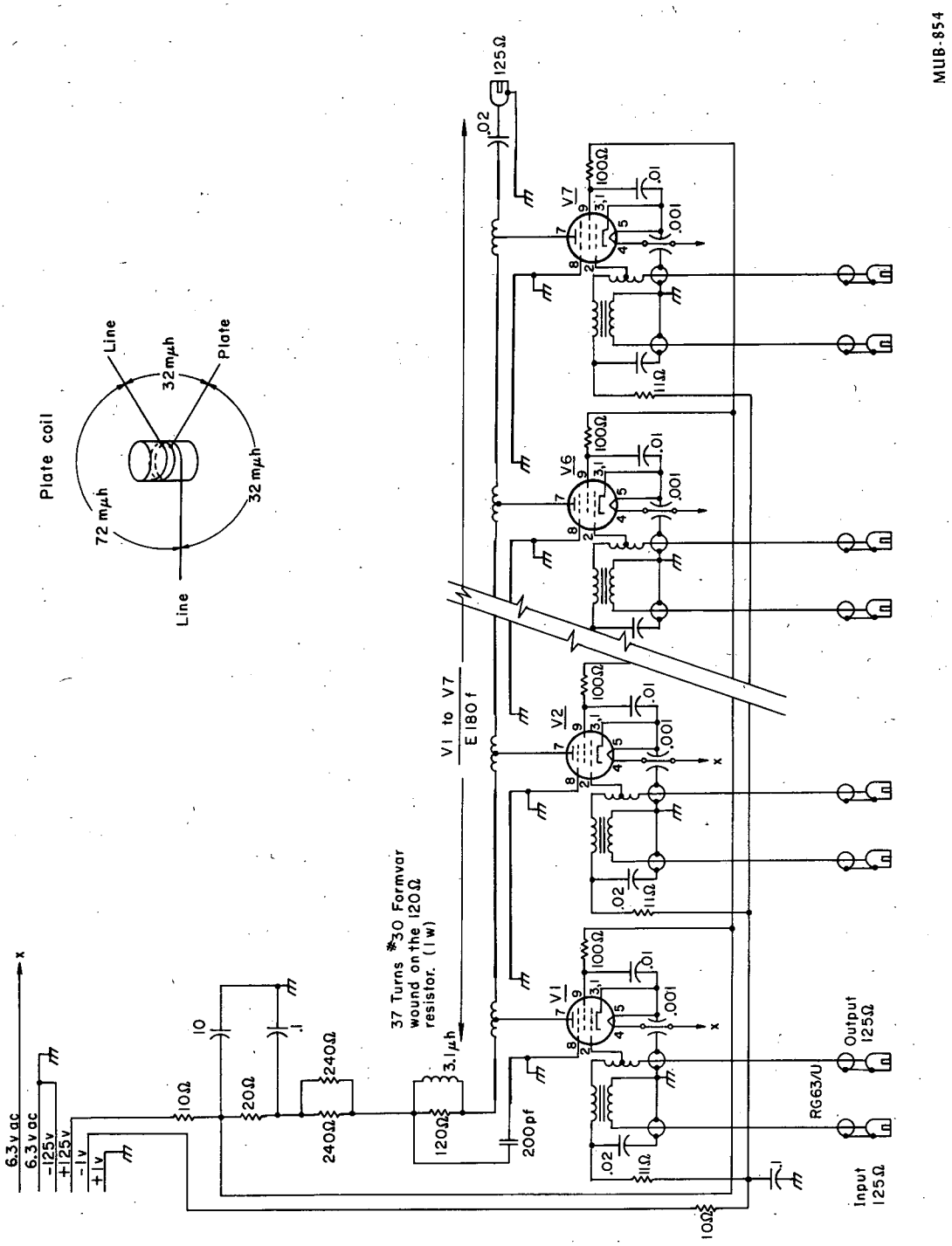

Fig. 6. Sevenfold adder circuit diagram.

added in two threefold adders similar to the sevenfold adder, and any combination of alternate tubes was required to satisfy the trigger requirement. The rate of accidental coincidences due to dark current in the six outer tubes was 800 counts/min with the refrigerator operating, a value lower by a factor of 10 than the real background due to the radioactivity of the surroundings. The refrigerator reduced the singles rate from individual tubes by a factor of six, on the average, from the room-temperature rate.

Delay Cables

The delay lines used to delay the γ counter signal consisted of two sections: (a) the trigger delay, labeled "$\pi\gamma$ delay" on the circuit diagram (Fig. 3), which utilized up to 3 μsec of 1-5/8-in. Prodelin coaxial cable,[9] (b) the oscilloscope γ signal cable, which consisted of approximately the same length of 2-in. Styrofoam-dielectric cable manufactured at the Lawrence Radiation Laboratory. In addition, during the slow-neutron runs at 67 feet, 1.1 μsec of Prodelin cable was used in the γ delay line. Two microseconds of delay cable attenuated the γ-signal pulse-height approximately 20%. The γ-signal cable was enclosed in a temperature-controlled room which maintained the temperature constant within $\pm$ 1°C, or the total time-delay constant within $\pm$ 0.04 nsec.

The delay of the cable used was measured with an artificial pulse designed to simulate the phototube output pulse. The cable-measuring circuit is shown in Fig. 7. The output of the driven pulser was split, and one pulse was displayed directly on a Hewlett-Packard dual trace sampling oscilloscope. The other pulse was displayed on the remaining trace after traveling through the unknown delay. The oscillator frequency was varied until the time between half heights of successive pulses was equal to the unknown delay time. In this condition the half heights of successive pulses coincide on the oscilloscope face. The change in the artificial pulse shape due to frequency-dependent attenuation in the delay line is equal to the change in the actual phototube pulse if the two pulses are identical. The degree to which this was achieved is discussed in the section on errors. The frequency needed to satisfy the above condition was measured with a

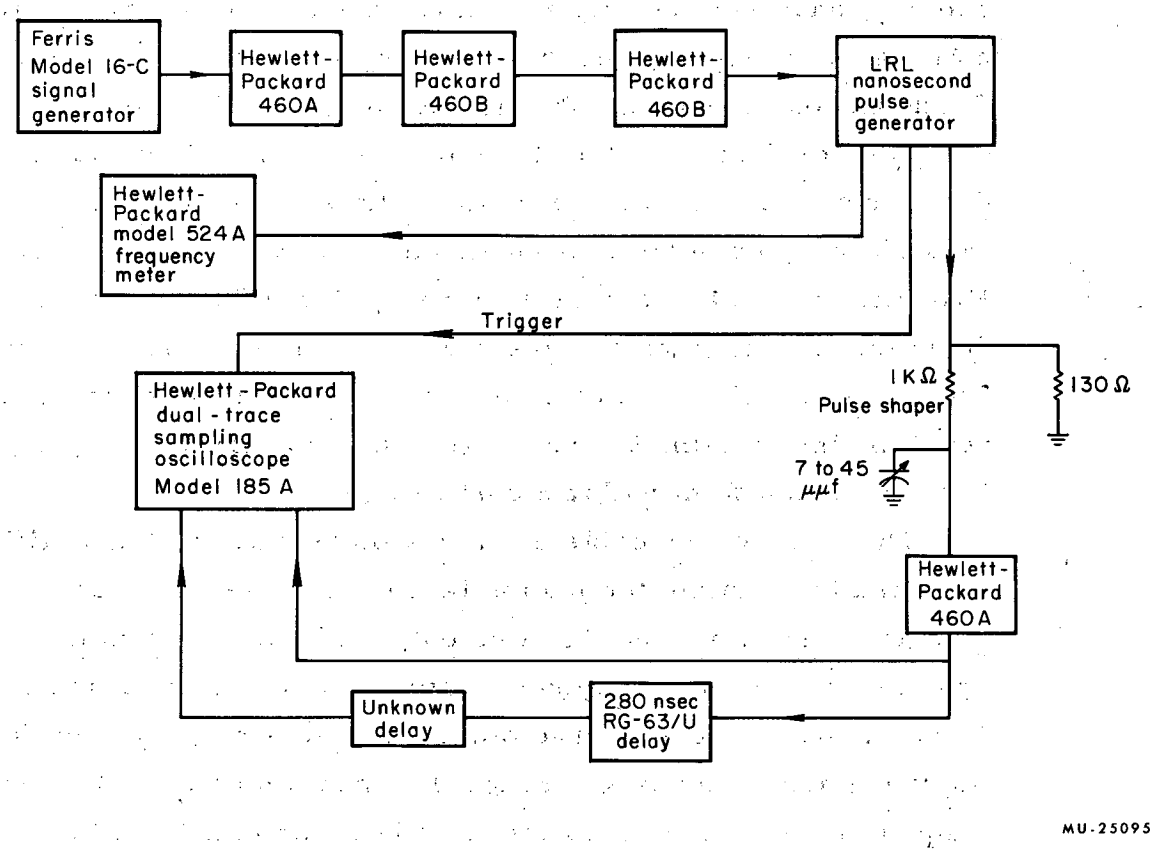

Fig. 7. Circuit diagram for delay measurement.

Hewlett-Packard 524A frequency meter, and the cable delay was given by the reciprocal of this frequency. Each cable was measured more than one time, and the rms deviation determined in this way was 0.05 nsec.

Measurement of Flight Path Length

The changes in flight path length were measured with a calibrated metal tape fastened to the neutron counter and used at constant tension and temperature. The tape correction factor at both positions used was found to be 0.999966 as determined from a standard tape obtained at the Lawrence Radiation Laboratory, Livermore California.

Long-Spill Meson Beam

At the 17-foot depth the main source of background in the neutron counter was proportional to the cyclotron beam intensity. In this condition, the signal-to-background ratio of the final data at a fixed beam intensity is proportional to the fractional spillout time of the meson beam. In order to maximize this ratio, the recently installed cyclotron auxiliary dee was utilized with which the duty cycle was increased from 3% to more than 50%. At depths greater than 30 feet, the background level in the neutron counter was essentially independent of the meson beam intensity.

Oscilloscope Calibration

The 517 oscilloscope was time-calibrated by photographing the amplified output of a sine-wave signal generator operating at 100.17 Mc and at 150.04 Mc. The sweep speed measured in this way was indeterminate to approximately 0.3% over the portion of the scope face used during the data taking. The results of this calibration are contained in Table I.

Neutron-Counter Magnetic Shielding

The magnetic shielding around the neutron counter reduced the field at the position of the photomultiplier tubes to less than 100 milligauss transverse to the axes of the tubes and to less than 150 milligauss along the axes of the tubes. The magnetic field varied from these upper limits to approximately zero depending upon the position of the neutron counter relative to the cyclotron. There were, however, no detectable changes in the operating characteris-

Table I. Oscilloscope sweep-speed calibration

At 6.6649 nsec/division		At 9.98304 nsec/division	
Division #	Distance on scanning machine (mm)	Division #	Distance on scanning machine (mm)
1	19.15	1	25.71
2	31.10	2	43.56
3	42.85	3	61.46
4	54.80	4	79.56
5	66.85	5	97.26
6	78.75	6	114.66
7	90.65	7	131.61
8	102.35	8	148.11
9	113.70	9	164.46
10	124.90	10	180.26
11	135.90	11	195.36
12	146.95	12	210.26
13	157.95	13	224.71
14	168.75	14	238.96
15	179.35		
16	189.65		
17	199.65		
18	209.55		
19	219.10		
20	228.67		
21	238.17		
22	246.92		

Note: The average position of the neutron signal half height is 139 mm.

The abscissa conversion factor in Figs. 11 to 18 is approximately 0.6 nsec mm.

tics of the photomultiplier tubes attributable to the magnetic field variation. The quantities measured accurately were transit-time spread and time delay. In addition, the pulse height was roughly determined and found to be constant.

Neutron-Counter Radiation Shielding

The shielding placed around the neutron-counter scintillator reduced by a factor of three (compared with the value obtained from a previous experiment[1]) that portion of the background not associated with beam intensity. At the same time, however, the efficiency of this counter for detecting background was increased by a factor of approximately three, so that the total shielding effect was a factor-of-nine reduction in background detection rate.

IV. RESOLUTIONS AND COUNTING RATES

The electronic resolution of the neutron counter was measured with the aid of a pulsed hydrogen discharge lamp installed in the scintillator. This light was pulsed at a rate of 300 times a second, with a pulse width of 2 nsec. The light intensity was adjusted to correspond to the measured slow-neutron pulse-height spectrum and then the output of the sevenfold adder was photographed along with a trigger signal taken from the pulser. The oscilloscope trace was triggered by a coincidence between any two alternate phototubes in the neutron counter. This requirement imposed the same restrictions on time jitter as those found during the data-taking runs. The measured time differences between pulser trigger signal and sevenfold output signal yield the intrinsic electronic resolution of the neutron counter. See Fig. 8 for the time distribution of this pulse-height range. The rms width was measured at 17 feet, 47 feet, and 67 feet in order to determine any change in this quantity with position. The rms deviation about the mean remained constant at $2.90 \pm .13$ nsec at these depths.

The resolution of the γ counter plus neutron counter system was measured by the simultaneous detection of the two γ rays from neutral pion decay. The electronic resolution of the neutron counter for γ-ray pulse height was measured as before, using the light pulser adjusted to yield the proper pulse-height range. See Fig. 9

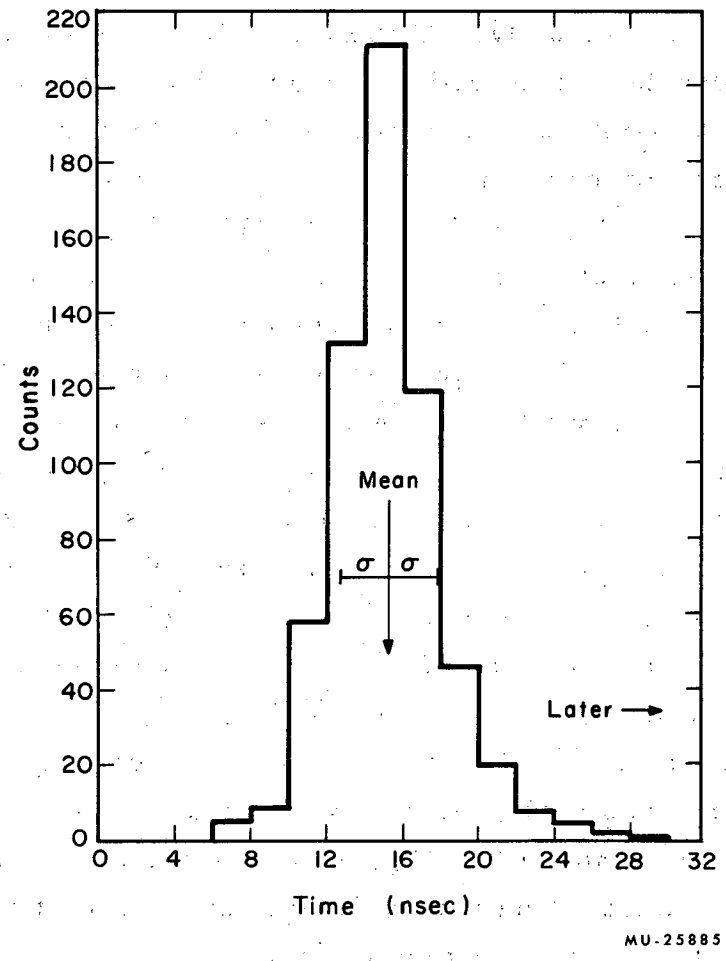

Fig. 8. Neutron counter resolution at 17 ft. ~~spectrum of~~ for slow-neutron pulse height.

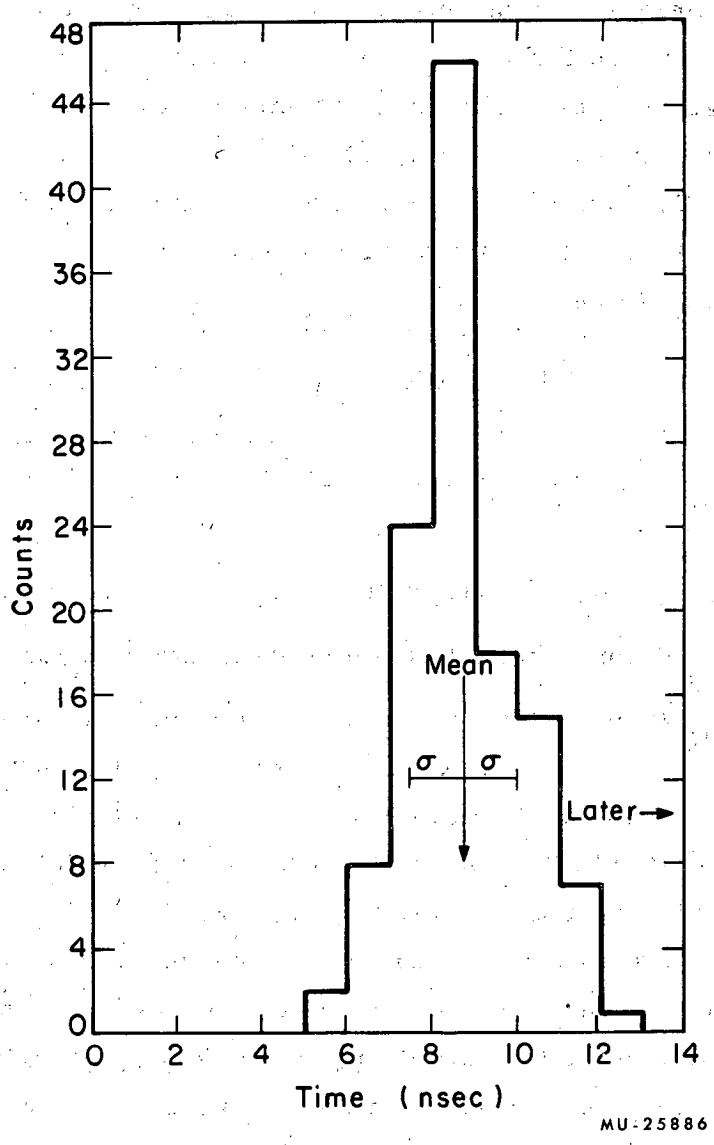

Fig. 9. Neutron counter resolution at 17 ft. ~~spectrum of~~ FOR π^0-decay γ pulse height.

for the time distribution of these larger pulses. The rms width for the neutron counter alone was 1.3±.08 nsec for this pulse-height range. The total γ resolution width was 2.8±.12 nsec, from which we find the intrinsic rms width of the γ counters alone to be 2.5 nsec for the pulse-height range of the slow-neutron runs.

The rms spread in the flight time of slow neutrons due to finite target height was calculated on the assumption of a pion beam uniform in intensity in the vertical direction striking the 1-in.-high liquid hydrogen target. The value obtained was 0.88 nsec. The same quantity for the 1-in.-thick plastic scintillator of the neutron counter was 0.82 nsec. By assuming Gaussian distributions, we find the total intrinsic resolution of the system for counting slow neutrons plus π^0-decay γ's ($\equiv \sigma_T$) to be

$$\sigma_T = \sqrt{\sigma_{\gamma T}^2 - \sigma_{n\gamma}^2 + \sigma_{nn}^2 + \sigma_{\text{target}}^2 + \sigma_{\text{scintillator}}^2}$$

or

$$\sigma_T = \sqrt{2.80^2 - 1.30^2 + 2.90^2 + 0.88^2 + 0.82^2} = 4.00 \pm .23 \text{ nsec},$$

where

$\sigma_{\gamma T} \equiv$ rms spread of the total system for counting π^0-decay γ,

$\sigma_{n\gamma} \equiv$ rms spread of the neutron counter for counting π^0-decay γ,

$\sigma_{nn} \equiv$ rms spread of the neutron counter for counting slow neutrons, and where we have used $\sigma_\gamma = \sqrt{\sigma_{\gamma T}^2 - \sigma_{n\gamma}^2} \equiv$ rms spread of the γ counters for counting π^0-decay γ's.

A numerical fold of the distributions from which $\sigma_{\gamma T}$ and σ_{nn} were obtained yields the result $\sigma_T = 4.13 \pm .23$ nsec.

A direct measurement of this quantity was made by the following technique: The total resolution of the system was measured for the simultaneous detection of the two π^0-decay γ's with the normal pulse-height range accepted from the γ counters. For the neutron counter, only those signals were accepted which yielded the slow-neutron pulse-height spectrum. The value obtained was $\sigma_T = 4.71 \pm 0.43$ nsec, which includes the artificial addition of the two terms σ_{target} and $\sigma_{\text{scintillator}}$. The value used in the following is $\sigma_T = 4.24 \pm .41$ nsec.

The beam intensity was measured with a 1×10-in. scintillation

counter placed at the position of the liquid hydrogen target center in coincidence with $\pi 1$ and $\pi 2$. In front of the small counter was placed 5 in. of carbon degrader to approximate the 7.5 in. of carbon used during the experiment. With the cyclotron running at reduced beam and with short target spill-out time, the average counting rate was $2.2 \times 10^7 \text{ min}^{-1}$ extrapolated to full beam intensity. This value corresponds to $2 \times 10^7 \text{ min}^{-1}$ in a 1×4-in. area. With the hydrogen target filled and in position, a range curve was taken by measuring the coincidence rate between the π counters and the γ counters as a function of degrader thickness. (See Fig. 10.) The full width at half maximum of this curve corresponded to an energy spread of 11 Mev before degradation, with the mean at 113 Mev. If all particles had traversed a full 12 inches of liquid hydrogen, 60% of the pions would have stopped in hydrogen. The accidental coincidence rate between the π monitor and the γ counters at the highest beam intensity was only 14% of the total $\pi\gamma$ rate; however, only 20% of the total $\pi\gamma$ rate was due to the presence of liquid hydrogen in the target.

The measured detection efficiency for those 400-kev neutrons which reached the neutron counter was 40%, which indicates that approximately 66% of the knock-on protons yielded a detectable light pulse. The measured detection efficiency for the 8.8-Mev neutrons was 22%, which corresponds to a light-pulse counting efficiency of 96% for either the carbon or hydrogen nuclei struck by the higher-energy neutrons. The slow-neutron detection rate at 17 feet extrapolated to full beam intensity was 4.5 neutrons per minute.

V. DATA AND ANALYSIS

Figures 11 through 16 show the time distributions obtained for 400-kev and 8.8-Mev neutrons. The abscissa represents the distance between half-heights of the γ-counter signal and the neutron-counter signal as read on the film scanning machine. Note that a larger abscissa corresponds to shorter flight times. The time scale varies from run to run depending upon the position of the data relative to the oscilloscope face, but was approximately 0.6 nsec/mm throughout. Table I contains the oscilloscope sweep speed calibration.

A determination of the velocity from the position of the mean

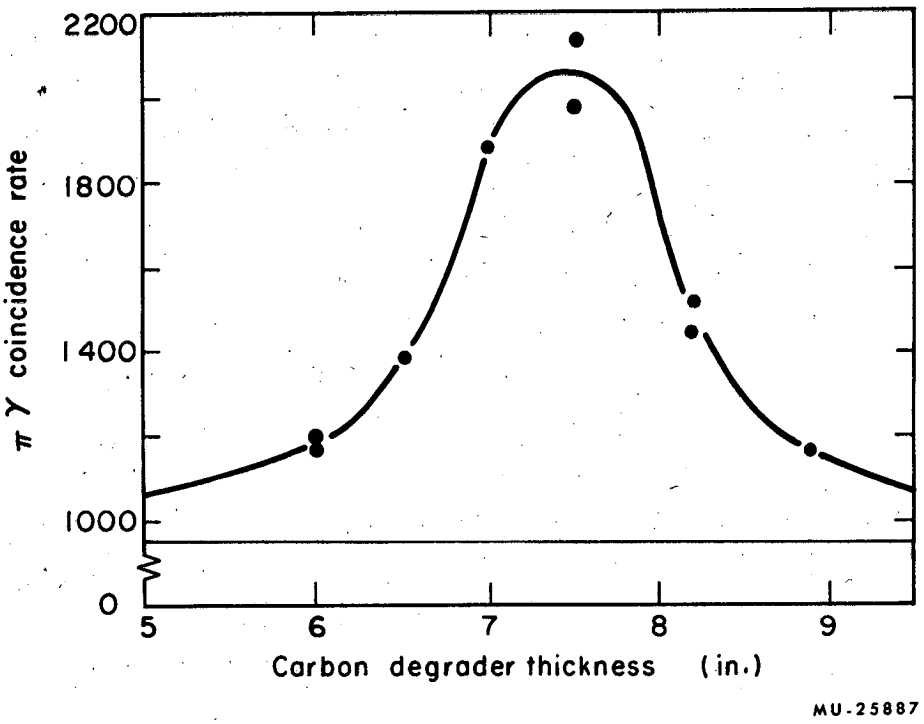

Fig. 10. Meson beam differential range curve; 1 in. of carbon equals 4.4 g/cm^2.

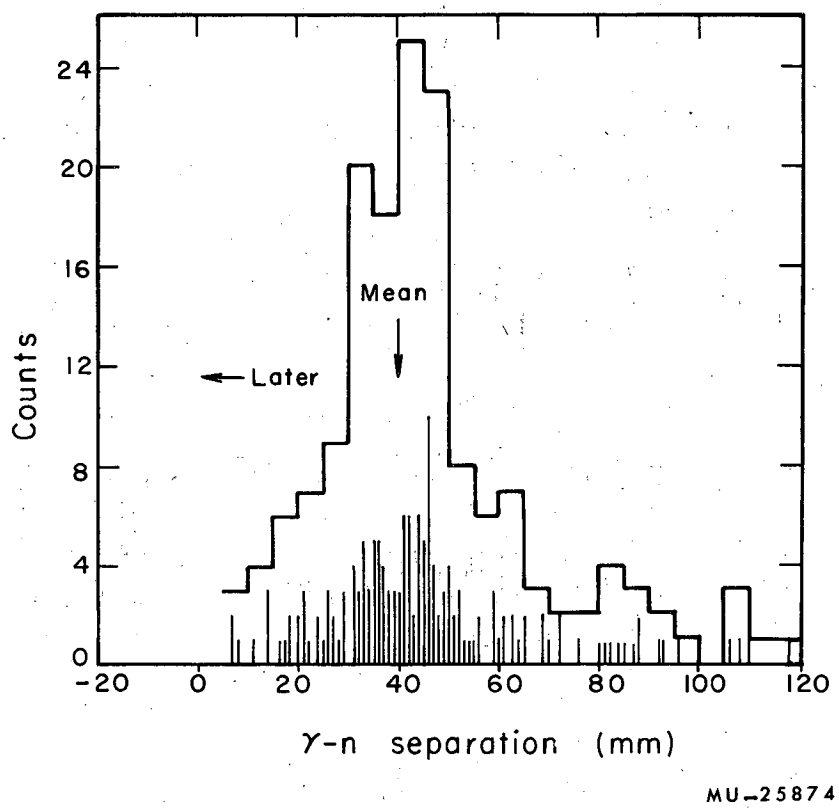

Fig. 11. Slow-neutron time distribution at 17 ft. NPH ≤ 0.8 max; γ PH ≥ 0.40 max. 0.630 nsec/mm at the position of the peak.

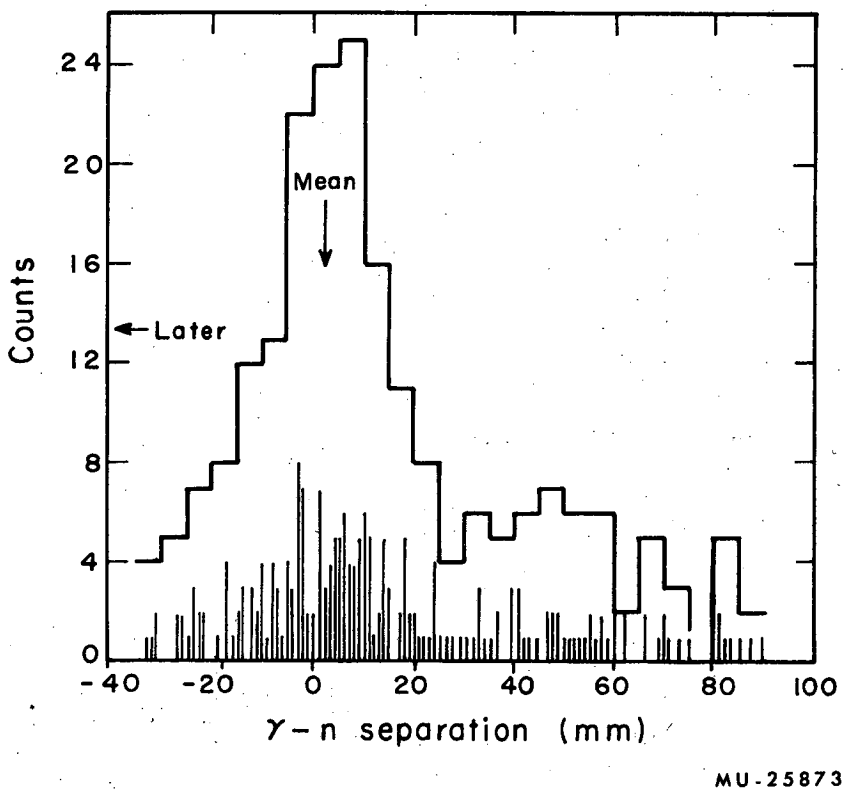

Fig. 12. Slow neutron time distribution at 17 ft. NPH ≤ 0.8 max; γ PH ≥0.40 max. 0.600 nsec/mm at the position of the peak.

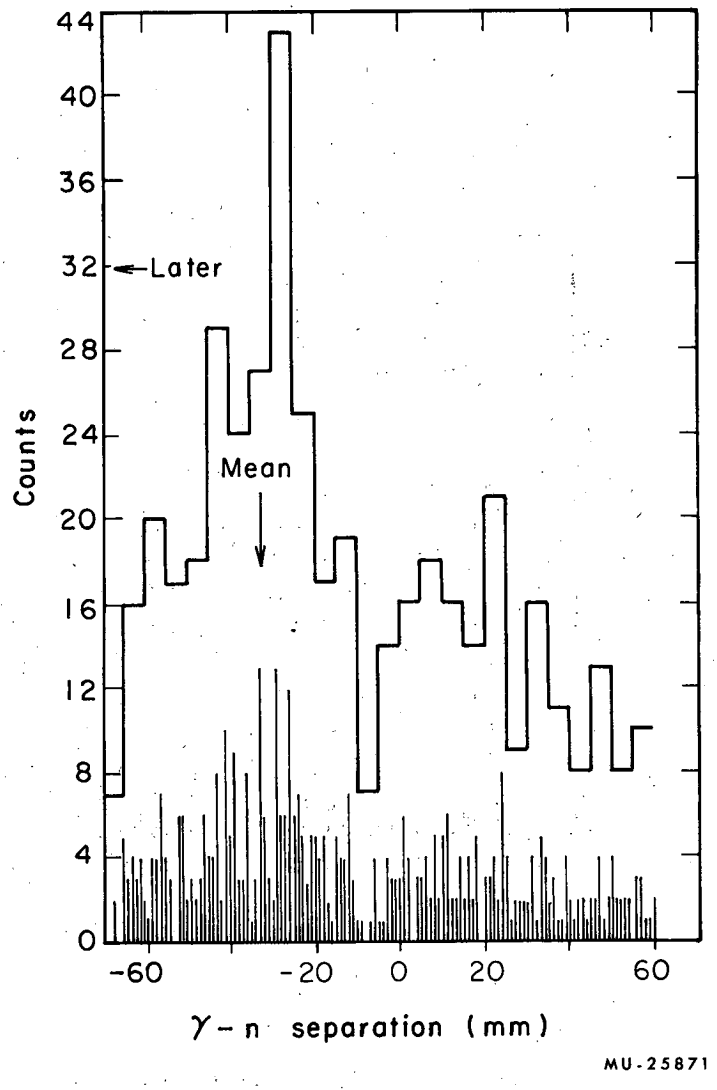

Fig. 13. Slow neutron time distribution at 47 ft NPH ≤ 0.8 max; γ PH ≥0.32 max. 0.571 nsec/mm at the position of the peak.

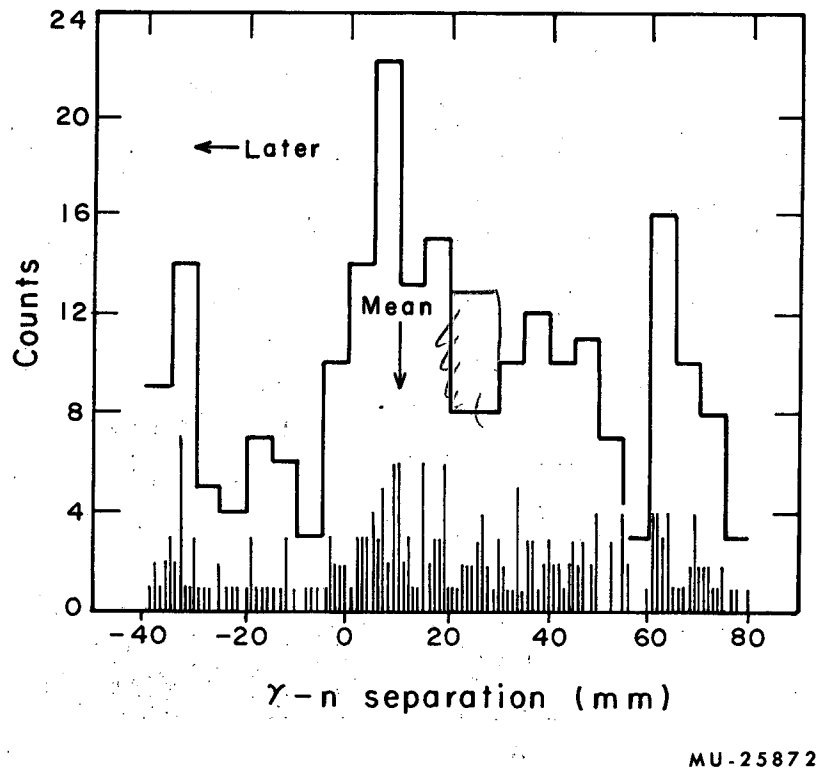

Fig. 14. Slow neutron time distribution at 67 ft. NPH ≤ 0.8 max; γ PH ≥ .32 max. 0.604 nsec/mm at the position of the peak.

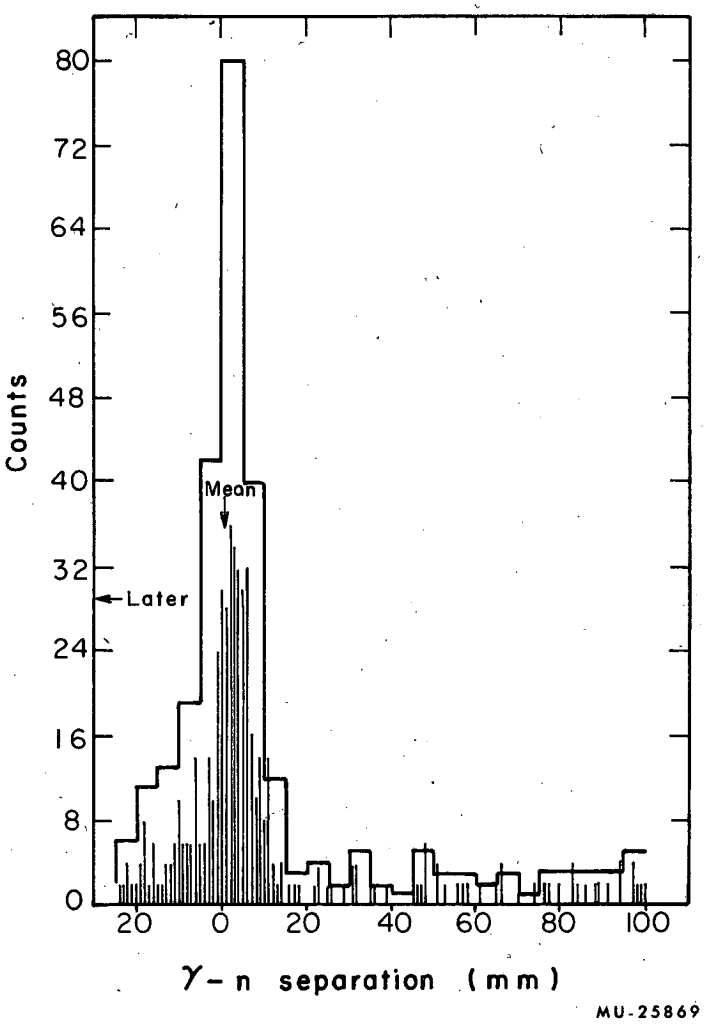

Fig. 15. Fast neutron time distribution at 17 ft. NPH ≥.92 max; γ PH ≥.50 max 0.600 nsec/mm at the position of the peak. The ordinate scale should be multiplied by one-half when referred to the ungrouped data.

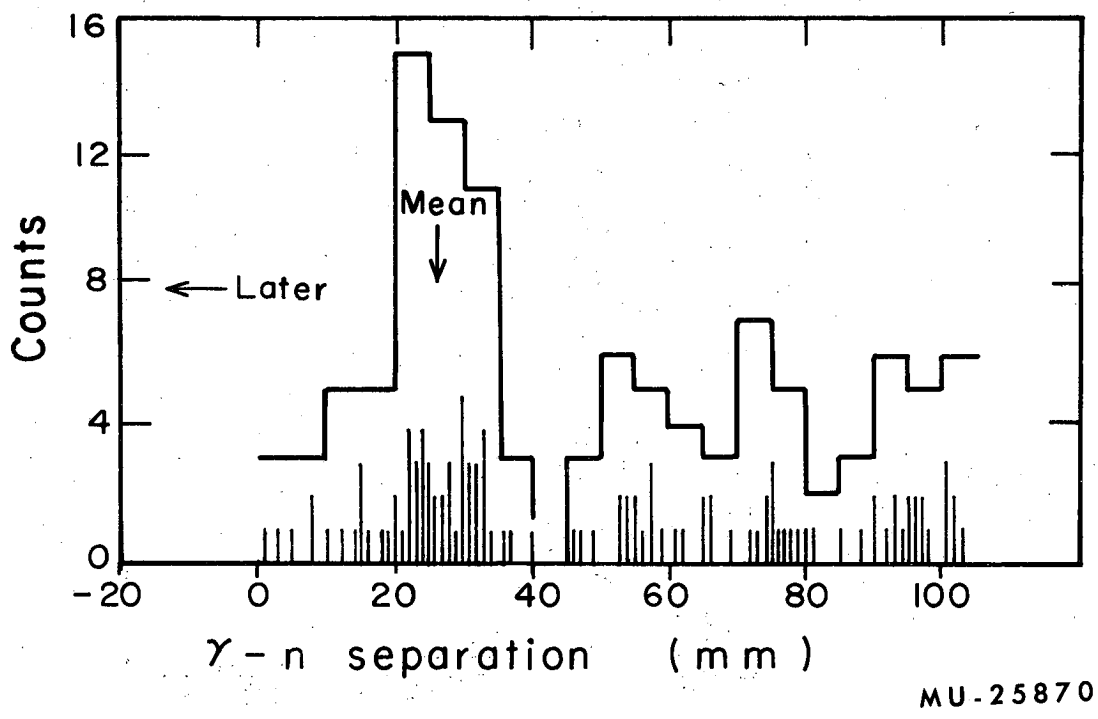

Fig. 16. Fast neutron time distribution at 67 ft. NPH ≥.92 max. γ PH ≥.46 max. 0.615 nsec/mm at the position of the peak.

at each depth depends upon changes in shape of the ~~velocity~~ TIME distribution with depth. The effect of any fixed asymmetry in the intrinsic resolution of the equipment is to shift all distributions measured by this equipment by precisely the same amount.[10] This holds true exactly only if the distribution is measurable over the complete range of the variable involved.

In the case of the 400-kev neutron, the rms deviation about the mean at 17 feet was found to be significantly larger than the σ_T given above. The assumption is made in analyzing the data that this added deviation is due to effects which yield a symmetrical velocity spread about the mean velocity. It is therefore assumed that all asymmetries arise from the shape of the intrinsic resolution of the equipment, that is, the distribution from which σ_T was obtained. The exception to the above symmetry which was considered and corrected for is that due to scattering of the neutrons in the target and in the atmosphere between target and counter.

Because of the unexpectedly large spread in the slow-neutron velocity, the complete time distribution was not measured at 47 ft and 67 ft. The resolution width of the oscilloscope trigger coincidence circuit was too narrow to cover the complete time range necessary. At 47 ft only the high-velocity side was recorded on film to the full extent of the distribution. The low-velocity side was recorded only 1/3 of the distance from the peak to the limit of the spread. At 67 ft the peak was centered within the data taken, but neither wing was fully recorded.

The evidence that the slow-neutron time spread increased with depth comes from the following observations:

(a) The time distribution as found from the light pulser data at 17 ft may be compared to the measured neutron distribution at the same depth. The effect of the velocity spread is the smallest at this depth, but the full distribution was recorded. This comparison is made in Section VIII.

(b) This same comparison may be made by using the data from the detection of the γ rays from π^0 decay instead of the light-pulser data. As discussed in Section IV, only the low-pulse-height signal is

accepted from the neutron counter in this comparison.

(c) A comparison of the expected rate of detection of slow neutrons at 47 ft (as calculated from the measured rate at 17 ft) may be made with the observed rate. Only one-third of the expected rate was found within a peak as narrow as that found at 17 ft. A determination of the velocity distribution at 47 ft must be made on the assumption that the data are symmetrical about the calculated mean velocity, since only the high-velocity side was recorded at this depth. These data, with the expected background, are shown in Fig. 17. The effect of the undetermined ratio of helium to air concentration is included with the statistical uncertainty in the error shown in the figure. The residual velocity spread at this depth is discussed in Section VIII. The signal-to-background ratio at 67 ft was too low to permit a similar determination.

(d) The expected background rate at 47 ft may be determined from the target-empty data. These data yielded an accurate determination of the background time distribution (see Fig. 18) and pulse height, but the background rate was too sensitive to the poorly known beam intensity for a useful result. The result agreed with the rate found in (c) above, but with a much larger uncertainty.

A calculation was made of the effect of the observed asymmetric resolution function upon the mean value of the velocity distribution. Since only part of the data was recorded at the lower depths, there is a shift in the observed mean compared with the 17-ft data, where the complete distribution is available. This calculation consisted in folding the measured intrinsic resolution function into a symmetric triangular velocity function. The mean was then calculated over the total distribution and also over the experimentally available portions. This permits a correction to be made to the data at the lower depths relative to the 17-ft data where the full distribution was recorded.

The technique used to determine the mean at all depths is the following: from the target-empty data it is known that the detection efficiency is constant within a 70-nsec time region. A fixed point is selected within the constant-efficiency region and to one side of the visible peak in the data. This fixed point remains one extreme of the region over which the mean is taken. The mean is then computed over an arbitrary

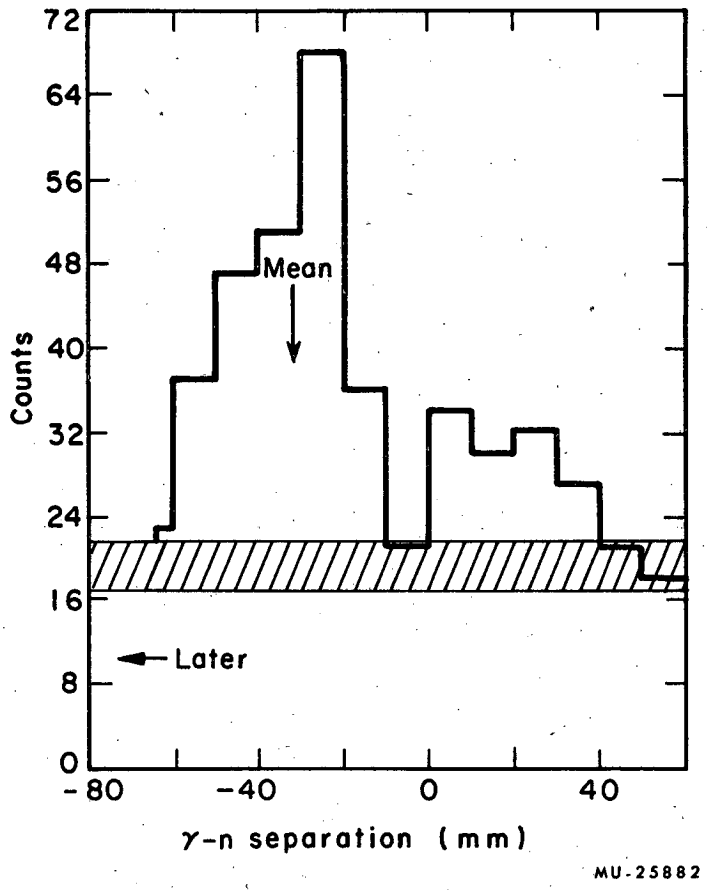

Fig. 17. Slow-neutron time distribution at 47 ft, with expected background; 0.571 nsec/mm at the position of the peak.

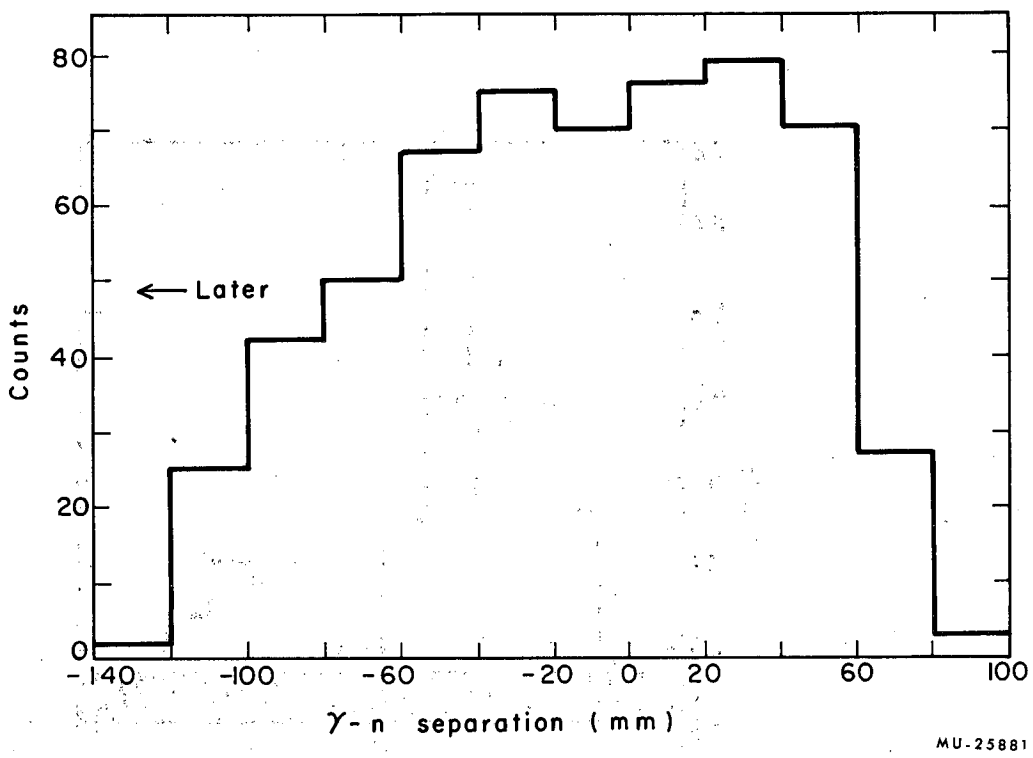

Fig. 18. Liquid hydrogen target-empty background time distribution; 0.600 nsec/mm at the center of the distribution.

portion of the constant-efficiency region which encompases the peak. A new region is then selected which is symmetrical about the computed mean and with the fixed point as one extreme. By repeating this process, a mean value is asymptotically arrived at which is centered within the region sampled. A uniform background was subtracted in all cases.

Figure 19 shows the neutron-counter pulse-height distribution in the region of the 400-kev neutron peak at 17 ft. The flat distribution from 0.1 to 0.8 maximum is taken as the knock-on proton pulse-height distribution. The cutoff at 0.1 maximum is due to scanner bias against the small, difficult-to-read pulses. A plot of the data with pulse height greater than 0.8 maximum gave no evidence of a peak in the time distribution and it is assumed to be background. The average signal-to-background ratio up to 0.8 maximum is 3.8 in this time region. Figures 20 and 21 show the pulse-height distribution, at two depths, of the background in the region of the slow-neutron peak. It is seen that some improvement in signal-to-background ratio is obtained by a high pulse-height cutoff. Figure 22 shows the γ-counter pulse height for counting the γ rays from π^0 decay. Some evidence of the expected peak is seen at 0.5 maximum. Figure 23, shows the target-empty background frequency (in the γ counter) vs pulse height. The pulse height in this figure has been attenuated by the delay cable to 0.60 that of the data in Fig. 22. Because of the lower average pulse height of the background, the final slow-neutron data were plotted for γ pulse heights greater than 0.40 maximum at 17 ft and 0.32 maximum at 47 ft and 67 ft. The reduction allows for the measured attenuation of the γ signals at the longer delays. Figures 24 and 25 show the γ-counter pulse heights from slow-neutron runs at 17 ft and 47 ft. The similarity to the known π^0-γ spectrum from Fig. 22 is evidence that real charge-exchange events are being detected. Figure 26 shows the γ-counter pulse-height spectrum from an 8.8-Mev neutron run. The pulse height, which is higher on the average than that seen in Fig. 22, is consistent with the factor-of-two difference in γ energy between these runs. Approximately one-fourth of the counts in Fig. 26 are due to background, and these lie predominantly below 0.4 maximum.

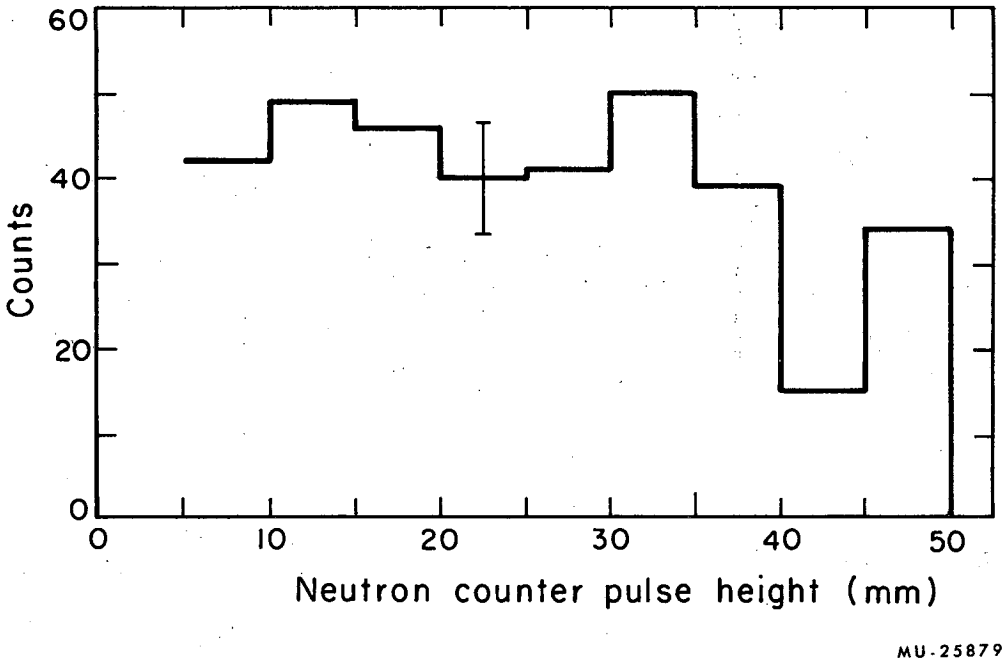

Fig. 19. Slow-neutron pulse-height distribution—neutron counter.

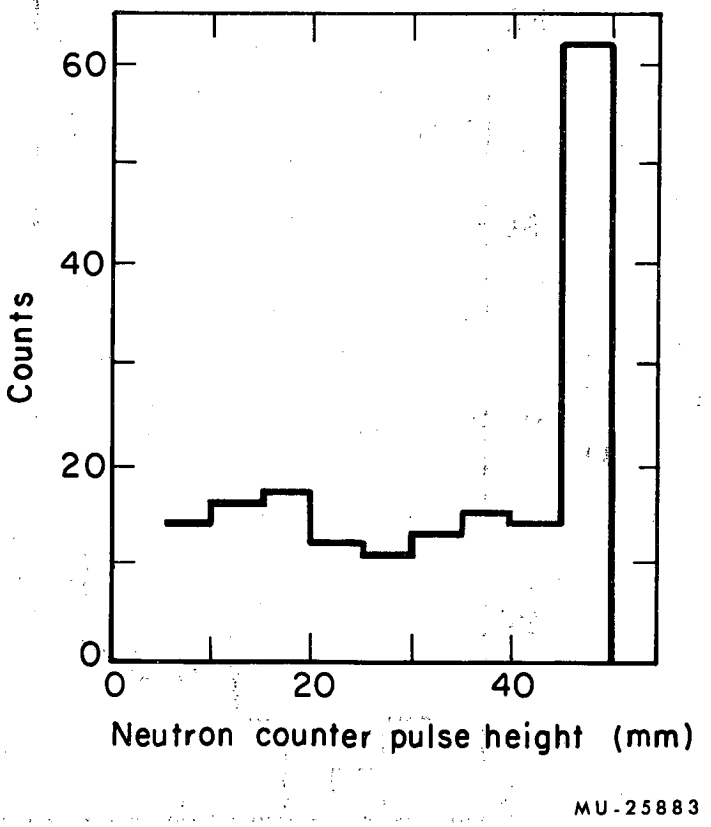

Fig. 20. Pulse-height distribution for slow-neutron counter background at 17 ft.

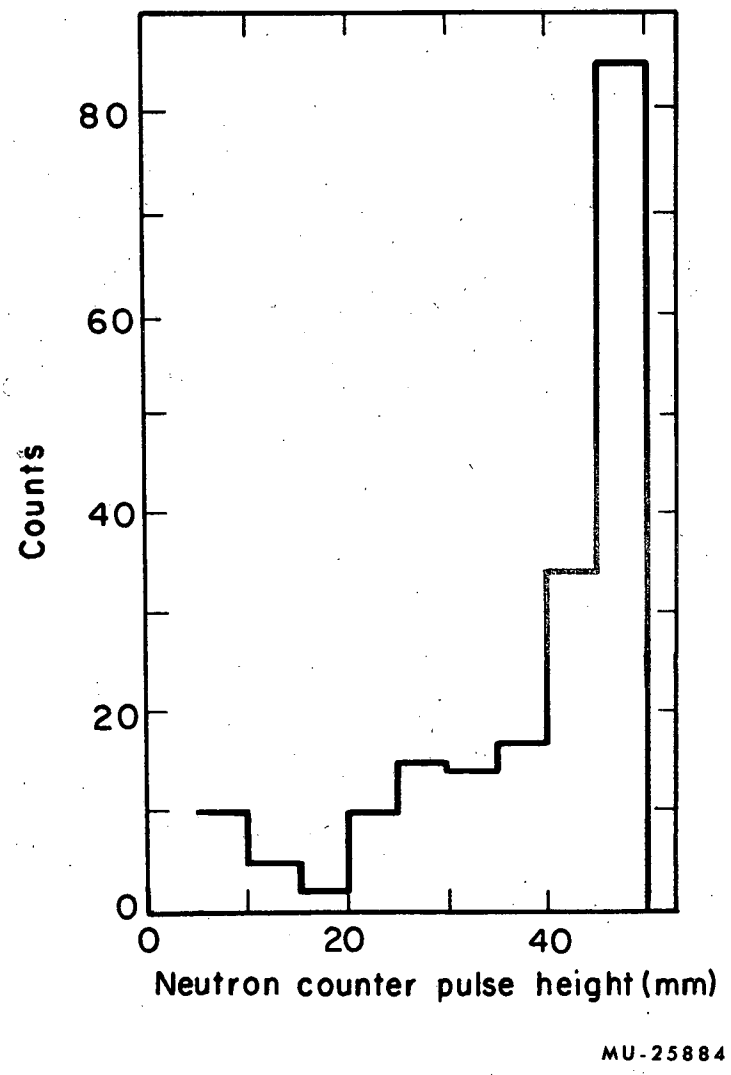

Fig. 21. Pulse-height distribution for slow neutron-counter background at 67 ft.

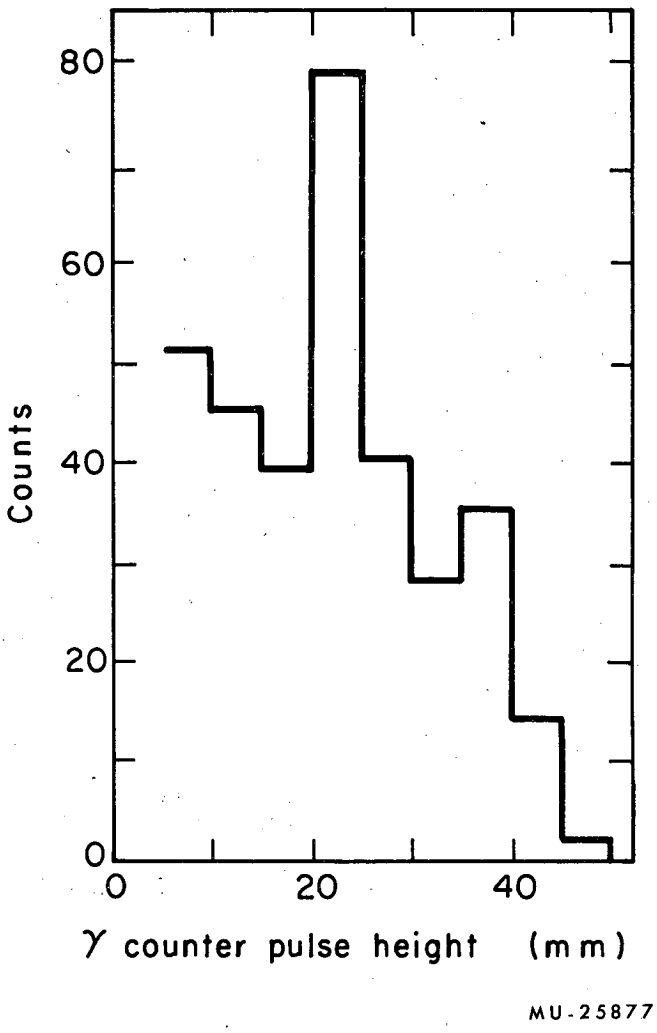

Fig. 22. Pulse-height distribution for gamma counter for π^0-decay γ's.

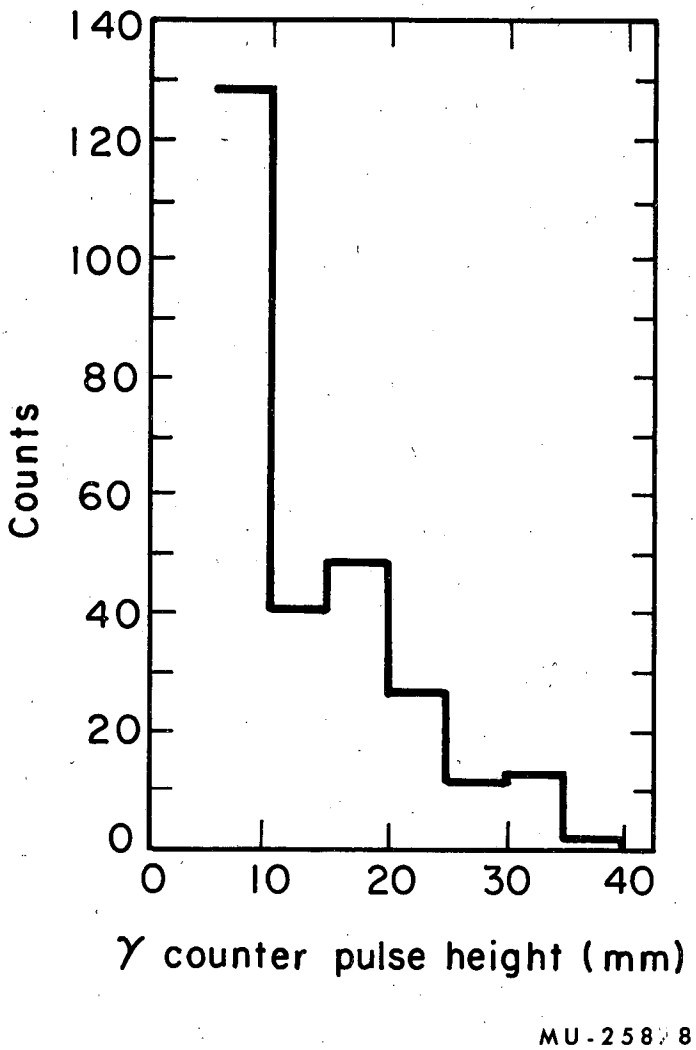

Fig. 23. Pulse-height distribution for gamma counter, target-empty background.

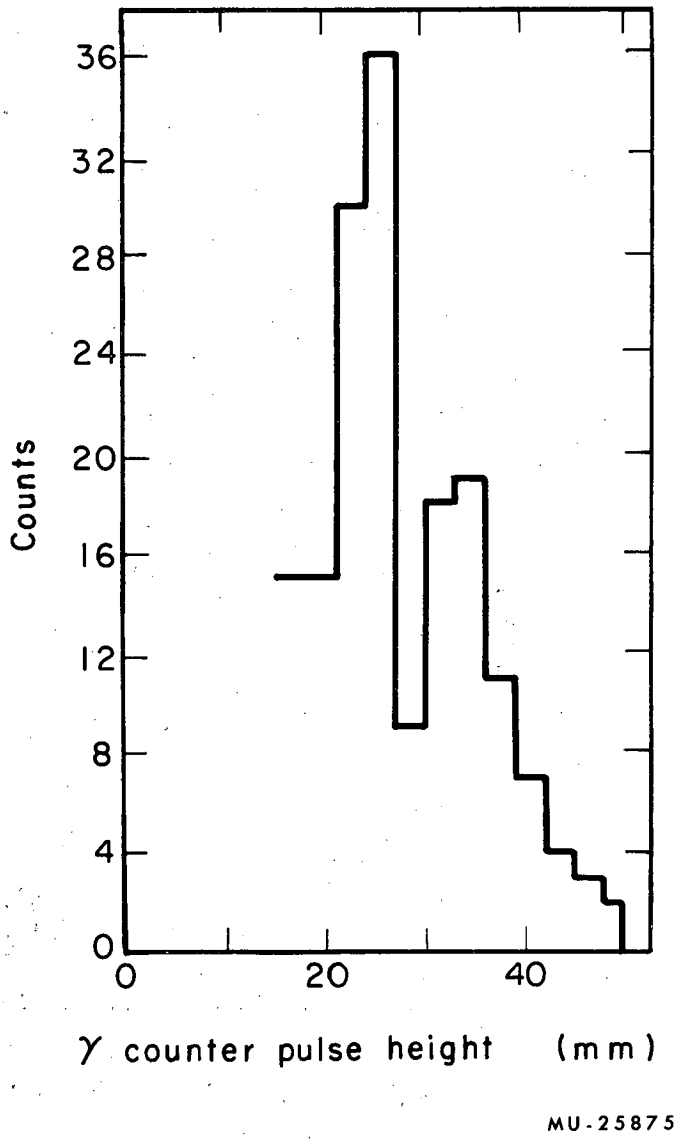

Fig. 24. Pulse-height distribution for gamma counter for π^0-decay γ's from slow-neutron run at 17 ft.

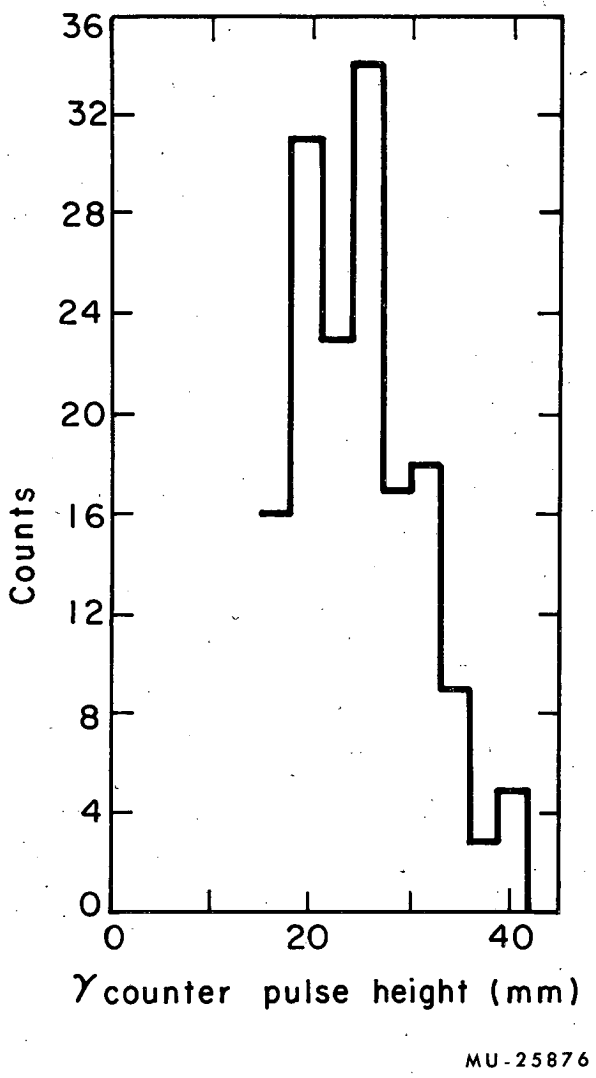

Fig. 25. Pulse-height distribution for gamma counter for π^0-decay γ's from slow-neutron run at 47 ft.

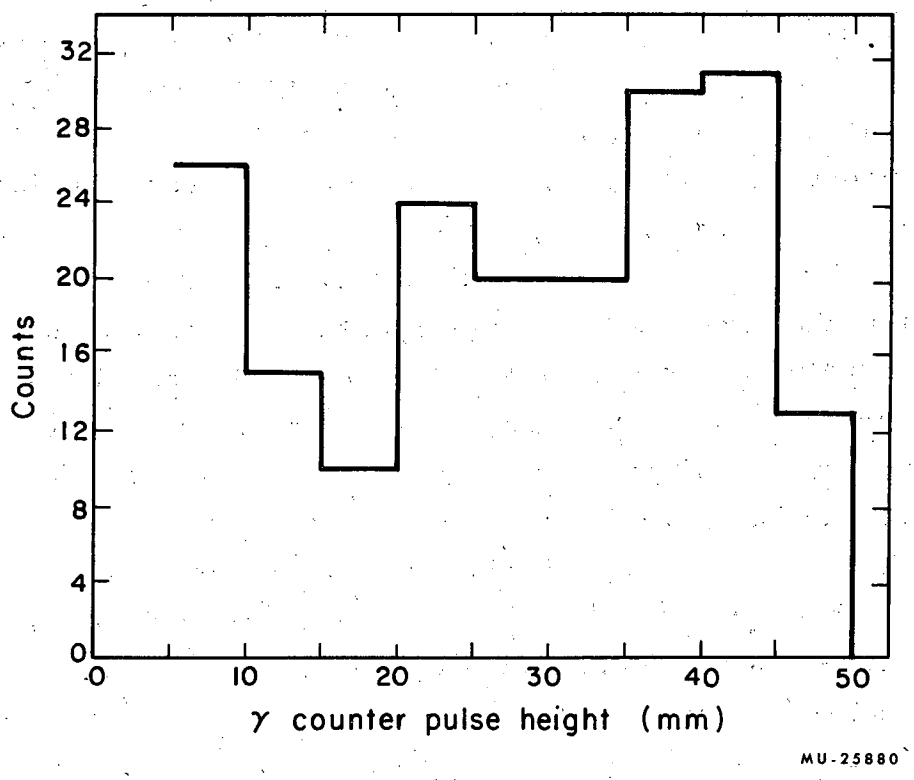

Fig. 26. Pulse-height distribution for gamma counter for 130-Mev γ's from fast-neutron run at 17 ft.

VI. CORRECTIONS AND ERRORS

The largest calculated correction to the observed data comes from the scattering of neutrons between source and detector. It was assumed in making this correction that all interactions in the liquid hydrogen, iron, aluminum, and air are elastic scattering events. At all depths the scattering from the hydrogen target structure, air, and hole walls resulted in a shift in mean flight time calculated to be less than 0.1 nsec. The calculated shift introduced by scattering from the liquid hydrogen is listed in Table II. Approximately 3% of the observed slow-neutron peak at 17 ft was due to neutrons scattered from hydrogen.

A calculation was made of the contribution to the spread in slow-neutron velocity due to pion-proton interactions in flight. At 90° to the incident pion beam, in the laboratory system, the velocity of slow neutrons from interactions in flight is lower than from interactions at rest. For a pion energy of 8 Mev, the neutron velocity is reduced 5%. For greater reductions than this, the neutrons will not be observed within the zero-pion-energy peak. The fraction of pions that interacted with 0 Mev $< T_{\pi} <$ 8 Mev was calculated to be less than 0.3% relative to the total number of interactions. Interactions in flight therefore have a negligible effect upon both the mean and the dispersion about the mean for the data obtained.

The correction labeled "Shift with depth" in Table II was obtained from the time of flight of the $\pi^0\gamma$ rays. The shift, which was $0.2 \pm .4$ nsec, is assumed to be independent of pulse height for values ranging from gamma pulse height to slow-neutron pulse height. The magnetic field at the position of the neutron counter phototubes was less than 100 milligauss transverse to the axes of the tubes, a value which results in less than 1% reduction in pulse height.

The correction to the delay measurement was made to compensate for the improper pulse shape of the pulse used to measure the delay cables. Each delay length was redetermined for various measuring pulse rise times, and the difference in delay length corresponding to the difference in rise time between real phototube pulses and artificial pulses is listed.

Table II. Summary of data and calculations.

Measured data	Units	400-kev neutron				8.8-Mev neutron		π^0 decay gamma			Ref.
		17 ft Run I	17 ft Run II	47 ft	67 ft	17 ft	67 ft	17 ft	47 ft	67 ft	Section
Delay	nsec	1054.77	1079.75	2055.27	2759.86	579.00	966.36	478.80	503.89	515.47	III
Tape[a]	ft	14.676	14.680	44.682	64.668	14.672	64.671	14.669	44.682	64.673	III
γ-n separation[b]	mm	+2.72	+40.23	-32.47	+10.06	+0.85	+25.66	+27.79	+18.83	+4.82	V
$\sigma_{\gamma\text{-n}}$[c]	nsec	6.35	6.88	5.63	3.46	3.94	2.47	3.26	3.17	3.49	V
Corrections											
Tape	ft	-0.0005	-0.0005	-0.0015	-0.0022	-0.0005	-0.0022	-0.0005	-0.0015	-0.0022	III
Scattering	nsec	-0.30	-0.26	-0.06	0	-0.10	-0.02	0	0	0	VI
Resolution Asymmetry	nsec	0	0	-0.03	-0.14	0	0	0	0	0	V
Shift with depth	nsec	0	0	+0.19	+.21	0	+.21	–	–	–	VI
Delay	nsec	0	0	+0.32	+0.32	+0.26	+0.23	+0.13	+0.13	+0.17	VI
Detection-efficiency change	nsec	+0.23	+0.14	0	0	+1.04	+0.74	+0.60	+0.33	+0.53	VI
Errors											
Delay reading	nsec	0.05	0.05	0.08	0.08	0.05	0.05	0.05	0.05	0.05	III
Tape reading	nsec	0.03	0.03	0.03	0.03	0	0	0	0	0	VI
γ-n separation	nsec	0.63	0.65	0.50	~~0.36~~ .60	0.28	0.46	0.21	0.32	0.25	VI
Scattering	nsec	0.10	0.10	0.05	0.05	0.03	0	0	0	0	VI
Resolution Asymmetry	nsec	0	0	0	0.05	0	0	0	0	0	V
Shift with depth	nsec	0	0	0.39	0.34	0	0.34	–	–	–	VI
Scope calibration[d]	nsec	0	0.07	0.06	0.02	0	0.04	0.04	0.04	0.01	III
Delay temp. change	nsec	0.01	0.01	0.03	0.04	0	0	0	0	0	VI
Detection-efficiency change	nsec	0	0	0.06	0.06	0	0.09	0	0.10	0.02	VI
γPH bias level	nsec	0	0	0.03	0.03	0	0.15	0	0	0	VI
Time-sampling region	nsec	0.06	0.06	1.42	0.27	0.06	0.27	0	0	0.06	VI

(a) Add 2.90 ft to tape reading to obtain actual separation between liquid hydrogen center and scintillator center.
(b) The separation is given in mm as read directly from the film-scanning machine.
(c) This value represents the standard deviation of the actual data used to calculate Δt.
(d) The error listed refers only to the error on the γ-n separation due to the uncertainty in sweep speed.

Note: All errors and corrections $\leq .01$ nsec are listed as "0".

The correction listed as "Detection-efficiency change" allows for the variation in detection efficiency as determined from the target-empty background runs. The correction was made by dividing the observed particle-detection rate by the relative efficiency, and recomputing the mean flight time. The error listed as "Tape reading" in Table II represents the flight time over one-fifth of a minor division on the calibrated tape.

The γ-n separation error is purely statistical and is given by the formula

$$\text{error} = \sigma_{\gamma\text{-}n}/\sqrt{N-1},$$

where N is the number of events used in computing the mean.

The error labeled "Delay temperature change" represents the change in delay time caused by a $\pm 1^{\circ}$C temperature variation in the temperature-controlled delay house.

The γ PH (pulse height) Bias Level error arises from the inability to determine precisely the γ PH attenuation vs delay length.

The "Time-sampling region" error arises from the uncertainty in the γ-n separation due to the unknown data-cutoff point. The error represents the rms shift in the γ-n separation as determined by calculating the separation for a range of cutoff points.

VII. CALCULATION OF PION MASSES

A. Mass Difference, $m_{\pi^-} - m_{\pi^0}$

If the binding energy between negative pions and protons is taken to be zero, then the pion mass difference is given by

$$\Delta \equiv m_{\pi^-} - m_{\pi^0},$$

$$\equiv m_{\pi^-} - [(m_{\pi^-} + m_p)^2 + m_n^2 - 2\gamma_n{}^s m_n (m_{\pi^-} + m_p)]^{1/2} \text{Mev}/c^2,$$

where

$\gamma_n{}^s = [1 - (\beta_n{}^s)^2]^{-1/2}$, $\beta_n{}^s$ is the velocity of the slow neutron in units of the velocity of light. From the work of Day et al.[11] and Russell and Shaw[12] on the capture time of pions in hydrogen it is found that negative pions undergo the strong interaction with protons from n levels greater than n = 2. Therefore the average binding energy is probably less than 360 ev. Since this number is small com-

pared with the other errors involved in the mass determination, it is set equal to zero in the calculation above. Another small correction, on the order of 50 ev (due to the finite π^--p center-of-mass velocity at the time of the interaction, as discussed in Section VIII), is also neglected.

The error on the mass difference is given by

$$S_\Delta = \frac{1}{m_{\pi^0}} [(m_{\pi^-} - \delta)^2 S_\delta^2 + (\Delta - \delta)^2 S_{m_{\pi^-}}^2 + (m_n[m_{\pi^-} + m_p] \beta_n^{s\,2})^2 (\frac{S_d^2}{d^2} + \frac{S_t^2}{t^2})]^{1/2} \text{ Mev/c}^2,$$

where $\delta = m_n - m_p$, d is the slow-neutron flight distance and t is the slow-neutron flight time. In this formula the approximation $\gamma_n^s = 1$ is used. Therefore

$$S_\Delta = [(1.024)^2 S_\delta^2 + (0.0237)^2 S_{m_{\pi^-}}^2 + (6.52)^2 (\frac{S_d^2}{d^2} + \frac{S_t^2}{t^2})]^{1/2} \text{ Mev/c}^2.$$

From Table II, the following information is obtained:

From 17 ft to 47 ft: $v_n^s = 0.0293838$ ft/nsec,

$\Delta = 4.6030$ Mev/c^2,

$S_\Delta = 0.0104$ Mev/c^2.

From 17 ft to 67 ft: $v_n^s = 0.0293997$ ft/nsec,

$\Delta = 4.6067$ Mev/c^2,

$S_\Delta = 0.0031$ Mev/c^2.

The weighted average of Δ is

$$\Delta = 4.6064 \pm .0030 \text{ Mev/c}^2.$$

B. Negative Pion Mass

If we again neglect the π^--p binding energy, we have

$$m_{\pi^-} = \gamma_n^F m_n (1 + \beta_n^F) - m_p \text{ Mev/c}^2,$$

where β_n^F is the velocity of the 8.8-Mev neutron in units of the velocity of light.

The error (squared) on the pion mass is

$$S^2_{m_{\pi^-}} = [(\gamma_n{}^F)^3 m_n (1 + \beta_n{}^F)(\beta_n{}^F)^2 + \gamma_n{}^F m_n \beta_n{}^F]^2 [\frac{S_d{}^2}{d^2} + \frac{S_t{}^2}{t^2}]$$

$$+ [\gamma_n{}^F (1 + \beta_n{}^F)]^2 S^2_{m_n} + S^2_{m_p} \quad (\text{Mev}/c^2)^2,$$

$$\text{or } S_{m_{\pi^-}} = [150^2 (\frac{S_d{}^2}{d^2} + \frac{S_t{}^2}{t^2}) + 1.14^2 S^2_{m_n} + S^2_{m_p}]^{1/2} \text{ Mev}/c^2.$$

From Table II we find

$$v_n{}^F = 0.134317 \text{ ft/nsec},$$

$$m_{\pi^-} = 139.69 \text{ Mev}/c^2,$$

$$S_{m_{\pi^-}} = 0.29 \text{ Mev}/c^2.$$

The values used in the above error calculations were

$$S_\delta = 0.4 \text{ kev}/c^2, {}^{13}$$

$$S_{m_{\pi^-}} = 56 \text{ kev}/c^2, {}^{6}$$

$$S_d = 0.001 \text{ ft},$$

$$S_{m_p} = 10 \text{ kev}/c^2, {}^{6}$$

$$S_{m_n} = 10 \text{ kev}/c^2. {}^{6}$$

VIII. SLOW-NEUTRON VELOCITY SPREAD

The evidence concerning the unexpectedly large spread in the slow-neutron velocity is tabulated in Section V. The most probable rms deviation due to the measuring equipment is shown in Section IV to be $\sigma_T = 4.24 \pm .41$ nsec. The values given for $\sigma_{\gamma\text{-}n}$ in Table II do not represent the best estimate of the experimentally observed deviation, but refer only to that quantity calculated for the actual data used to obtain Δt. In order to obtain the best estimate of the observed deviation at the 17-ft position, σ was calculated by using only the "fast" half of the data and including the background region.

As the time region over which σ is calculated increases from zero, σ increases throughout the region of the velocity peak and then assumes an approximately constant value when the background region is included. The average of this approximately constant value from runs I and II at the 17 ft position is $\sigma_{17\,ft} = 6.18 \pm .50$ nsec. From this we find the residual rms deviation to be $\sigma_{R17\,ft} = 4.49 \pm .79$ nsec. The error includes the intrinsic statistical error from each calculated value of σ plus the observed rms deviation caused by the unknown signal cutoff point.

The residual rms deviation at 47 ft was found to be $\sigma_{R47\,ft} = 17.6 \pm 1.6$ nsec, where the error includes both the statistical uncertainty and that due to the uncertain background. The ratio of the residual deviation at 47 ft to that at 17 ft is $3.92 \pm .77$. The ratio of the target-to-counter distances at these two positions is 2.71. These ratios are in reasonable agreement with the hypothesis that the observed spread is due to effects originating in the hydrogen target.

The possible explanations for the observed residual deviation are listed below along with their expected magnitudes.

a. Variation in flight path due to finite target and scintillator size. This effect varies from approximately $\sigma = 0.5$ nsec at 17 ft to $\sigma = 0.2$ nsec at 47 ft, and therefore is of the wrong sign and too small to explain the observed effect.

b. Slow-neutron scattering. At the 17-ft position the correction of the data for scattering reduces the rms deviation by 0.23 nsec.

c. Unknown π^--p binding energy. If it is assumed that the pion is captured by the proton from an n level greater than or equal to 3,[10] then the maximum possible variation in binding energy is 360 ev. This corresponds to a maximum variation in flight time at 17 ft of 0.03 nsec.

d. Neutral-pion mean life. The present value of the π^0 mean life is $(1.9 \pm .5) \times 10^{-16}$ sec.[14] This value corresponds to an uncertainty in the time of flight of slow neutrons over a 50-ft flight path of less than .01 nsec.

e. π^--p thermal motion. The thermal velocity of hydrogen atoms in the liquid state was calculated under the assumption that the liquid and solid states would have the same velocity distribution at the same temperature.[15] From the Debye theory of specific heat combined with an

expression[16] for the rms amplitude of thermal vibrations, we obtain a value for the maximum thermal velocity of 1.2×10^5 cm/sec, which corresponds to a time spread of 0.08 nsec at 17 ft and 0.21 nsec at 47 ft.

f. Radiative de-excitation of the π^-p atom. The maximum velocity that the π^-p atom can attain from the recoil due to radiative de-excitation is 9×10^4 cm/sec, and is probably less than 1×10^4 cm/sec. This yields a negligible time spread at all depths.

g. Collisional de-excitation of the π^-p atom. The remaining process capable of explaining the large observed velocity spread is the process investigated by Day et al.[11] and Russell and Shaw.[12] They find that the experimentally observed π^- capture time[17] can be explained in terms of the slowing-down process described by Wightman[18] with the addition of Stark-effect reshuffling of the ℓ levels for n values of 3 to 5. This latter process is very fast compared with radiative de-excitation, and brings about the capture of π^- mesons in S states of principal quantum numbers 3 to 5. In the calculations above, the authors assumed a velocity of the π^--p system of 10^5 to 10^6 cm/sec as obtained from estimates of the collisional de-excitation energy. According to Day[19] velocitites of 10^7 cm/sec are completely compatible with the experimental results of π^- capture times and with the theoretical results of the slowing-down process.

The weighted average of the residual rms velocity spread as observed in this experiment is $(8.0\pm{}^{1.5}_{.7})\times10^6$ cm/sec. The last effect (item g) is believed to be the only one capable of explaining the large observed velocity spread.

IX. SUMMARY

1. The $m_{\pi^-}-m_{\pi^0}$ is $4.60^{56}_{64} \pm .00^{55}_{30}$ Mev/c^2, based upon the following assumptions:

a. The spatial distribution of stopping pions in the liquid hydrogen did not change with time.

b. The average time from initiation of events to their detection did not vary with time. Such a variation could be brought about by changing photomultiplier tube voltages. During the runs at 67 ft, one tube in the neutron counter was turned off. This could yield a shift of up to 0.2 nsec, which corresponds to one-fourth of a standard deviation

shift in flight time.

c. The observed spread in slow-neutron velocities was symmetrical about the calculated mean. If the observed spread in velocity is due to center-of-mass motion of the π^-p system, there is a corresponding negligible shift in the flight time from the at-rest value.

d. The frequency-meter crystal used in the delay-length determinations did not vary during these determinations more than the total long-term variation observed for this crystal. The observed variation corresponded to less than 0.01 nsec.

e. The strong interaction between pion and proton occurred from bound atomic n levels greater than 2.

2. The m_{π^-} is $139.69 \pm .29^{.41}$ Mev/c^2 based upon assumptions a, b, d, and e.

3. The rms deviation about the mean slow-neutron velocity corresponds to a rms velocity of the π^--p system of $(8.0 \pm {}^{1.5}_{.7}) \times 10^6$ cm/sec, with a distribution as shown in Fig. 17. This distribution includes the resolution function of the measuring equipment and the spatial distribution of the center-of-mass velocity.

ACKNOWLEDGMENTS

I would like to thank in particular Professor Kenneth M. Crowe for the valuable guidance and assistance offered by him throughout this experiment and during the author's graduate career.

In addition, a great deal of the original work with the equipment used in this experiment was done by Professor Roy P. Haddock, and his active interest until completion is greatly appreciated. Professor Alexander Abashian provided invaluable help during the running of the experiment with little thought of reward. His help and that of Mr. James Ryan were received with gratitude. The outstanding interest and completely dependable help offered by Reverend John L. Whitsell during the period he spent as a technician at the Radiation Laboratory were a source of inspiration to all concerned.

I would like to thank my wife for the great amount of patient understanding and sacrifice offered throughout my graduate career.

The members of the cyclotron crew under the supervision of Mr. James T. Vale and Mr. Lloyd B. Hauser performed their tasks with their usual reliablility.

This work was done under the auspices of the U. S. Atomic Energy Commission.

REFERENCES

1. M. Gettner, L. Holloway, D. Kraus, K. Lande, E. Leboy, and W. Selove, Phys. Rev. Letters 2, 471 (1959); W. Selove and M. Gettner, Phys. Rev. 120, 593 (1960); P. Hillman, W. C. Middlekoop, T. Yamagata, and E. Zavattini, Nuovo cimento 14, 887 (1959); R. Haddock, A. Abashian, K. Crowe, and J. Czirr, Phys. Rev. Letters 3, 478 (1959).
2. J. Kuehner, A. W. Merrison, and S. Tomabene, Proc. Soc. (London) (to be published).
3. W. Chinowsky and J. Steinberger, Phys. Rev. 93, 586 (1954); J. M. Cassels, D. P. Jones, P. G. Murphy, and P. L. O'Neill, Proc. Phys. Soc. (London) 74, 92 (1959).
4. W. H. Barkas and A. H. Rosenfeld, Data for Elementary-Particle Physics, UCRL-8080-Rev., Oct. 1, 1961. The error of ± 0.05 Mev/c^2 is the best estimate of the error on the mass difference measured by Haddock et al., Phys. Rev. Letters 3, 478 (1959). The error of ± 0.01 Mev/c^2 quoted by Barkas and Rosenfeld refers to a measurement by the same authors which was subject to larger systematic errors.
5. W. H. Barkas, W. Birnbaum, and F. M. Smith, Phys. Rev. 101, 778 (1956).
6. Cohen, Crowe, and Dumond, Fundamental Constants of Physics (Interscience Publishers, Inc., New York, 1957).
7. K. M. Crowe and R. H. Phillips, Phys. Rev. 96, 470 (1954).
8. For a description of equipment see the Lawrence Radiation Laboratory Counting Handbook, UCRL-3307 Rev., Jan. 1, 1959.
9. Manufactured by Prodelin, Inc., Kearny, New Jersey. This cable has an impedance of 125 ohms and an attenuation at 100 Mc of 3 db per 1000 ft.
10. K. M. Crowe, Precision Measurement of the Negative Pion Mass from its Radiative Absorption in Hydrogen, UCRL-2050, Dec. 18, 1952. (Thesis, unpublished).
11. T. B. Day, G. A. Snow, and J. Sucher, Phys. Rev. Letters 3, 61 (1959); and University of Maryland Physics Department Technical

Report No. 159; T. B. Day, Report No. 175; G. A. Snow, Report No. 196 (unpublished reports).

12. J. E. Russell and G. L. Shaw, Phys. Rev. Letters 4, 369 (1960).
13. R. O. Bondelid, J. W. Butler, C. A. Kennedy, and A. del Callar, Phys. Rev. 120, 887 (1960).
14. R. G. Glasser, N. Seeman, and B. Stiller, Phys. Rev. 123, 1014 (1961).
15. I. I. Frenkel, Kinetic Theory of Liquids (The Clarendon Press, Oxford, 1946), pages 93-98.
16. R. W. James, The Optical Principles of the Diffraction of X-rays (Bell, London, 1948), page 220.
17. T. H. Fields, G. B. Yodh, M. Derrick, and J. G. Fetkovich, Phys. Rev. Letters 5, 69 (1960).
18. A. S. Wightman, Phys. Rev. 77, 521 (1950); and Ph. D. Thesis (unpublished), Princeton University, 1949.
19. T. B. Day (University of Maryland, College Park, Maryland), private communication.